Author Manuscript

Author Manuscript

Author Manuscript

Author Manuscript

HHS Public Access

Author manuscript

*J Org Chem*. Author manuscript; available in PMC 2022 July 28.

Published in final edited form as:

*J Org Chem*. 2022 May 20; 87(10): 6742–6759. doi:10.1021/acs.joc.2c00449.

# Synthesis and Characterization of Bimetallic Nanoclusters Stabilized by Chiral and Achiral Polyvinylpyrrolidinones. Catalytic C(sp$^3$)-H Oxidation

**Huafang Fan**[1], **Zongbo Tong**[1], **Zhaoyang Ren**[1], **Kanchan Mishra**[1], **Shunya Morita**[1], **Edruce Edouarzin**[1], **Lingaraju Gorla**[1], **Boris Averkiev**[1], **Victor W. Day**[2], **Duy H. Hua**[1,*]

[1]Department of Chemistry, Kansas State University, Manhattan, Kansas 66506, U. S. A.

[2]Department of Chemistry, University of Kansas, Lawrence, KS 66045, U. S. A.

## Abstract

Second-generation chiral substituted poly-*N*-vinylpyrrolidinones (CSPVPs) (−)-**1R** and (+)-**1S** were synthesized by free-radical polymerizations of (3a*R*,6a*R*)- and (3a*S*,6a*S*)-5-ethenyl-tetrahydro-2,2-dimethyl-4*H*-1,3-dioxolo[4,5-c]pyrrol-4-one, respectively, using thermal and photochemical reactions. They were produced from respective *D*-isoascorbic acid and *D*-ribose. In addition, chiral polymer (−)-**2** was also synthesized from the polymerization of (*S*)-3-(methoxymethoxy)-1-vinylpyrrolidin-2-one. Molecular weights of these chiral polymers were measured using HRMS and the polymer chain tacticity was studied using $^{13}$C NMR spectroscopy. Chiral polymers (−)-**1R**, (+)-**1S**, and (−)-**2** along with poly-*N*-vinylpyrrolidinone (PVP, MW 40K) were separately used in the stabilization of Cu/Au or Pd/Au nanoclusters. CD spectra of the bimetallic nanoclusters stabilized by (−)-**1R** and (+)-**1S** showed close to mirror-imaged CD absorption bands at wavelengths 200 – 300 nm, revealing bimetallic nanoclusters' chiroptical responses are derived from chiral-polymer encapsulated nanomaterials. Chemo-, regio- and stereoselectivity were found in the catalytic C-H group oxidation reactions of complex bioactive natural products, such as ambroxide, menthofuran, boldine, estrone, dehydroabietylamine, 9-allogibberic acid, and sclareolide, and substituted adamantane molecules, when catalyst Cu/Au (3:1) or Pd/Au (3:1) stabilized by CSPVPs or PVP and oxidant $H_2O_2$ or *t*-BuOOH were applied. Oxidation of (+)-boldine *N*-oxide **23** using NMO as an oxidant resulted 4,5-dehydroboldine **27** and oxidation of (−)-9-allogibberic acid yielded C6,15 lactone **47** and C6-ketone **48**.

## Graphical Abstract

*Corresponding Author: duy@ksu.edu.

**Supporting Information**. This material is available free of charge via the Internet at http://pubs.acs.org.

The authors declare no competing financial interest.

Author Manuscript Author Manuscript Author Manuscript Author Manuscript

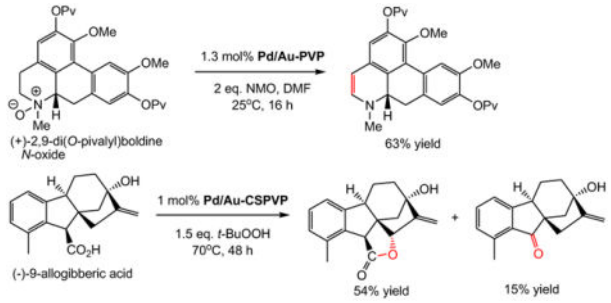


## INTRODUCTION

The application of catalysts and environmentally friendly chemicals such as bimetallic nanoclusters Cu/Au or Pd/Au in C($sp^3$)-H oxidation of natural products and complex compounds, leading to bioactive molecules, may contribute to a part of the solutions for climate challenge. The rise of global population increases demands of energy, food, health care, transportation, etc. Catalysts enhance the rates of reactions by lowering their activation energies compare with those of uncatalyzed reactions, thereby a reduction of energy and lesser or cheaper reagents are needed.[1] Late-stage C-H oxidation of complex bioactive molecules may provide pharmaceutical and fine chemical industries a greener and efficient process. Bimetallic nanoclusters require a stabilizer to maintain their nano-size structure. In addition to achiral stabilizers, chiral stabilizers have been explored for various possible applications. Chiral ligands,[2] chiral surfactants,[3] chiral DNA templates,[4] and chiral polymers[5a] have been used to produce nanoclusters in which the metal atoms, such as gold or palladium, may organize into nano-sized asymmetrical structures. Chiral nanoclusters have been investigated in asymmetric catalysis,[2a,5] chiral recognition,[6] and chiroptics.[7] Chiral gold or palladium nanoclusters have been reported,[2] and the studies of chiral polymers and polymeric chiral catalysts have progressed steadily in recent years.[8,9] The synthesis of bimetallic nanoclusters encapsulated by chiral substituted poly-*N*-vinylpyrrolidinones (CSPVPs) has been reported, but the application is still in its infancy.[5a] We investigate PVP-based polymers, possessing solubilities in both water and organic solvents[10] for encapsulation of bimetallic nanoclusters and catalytic oxidation reactions. The amide functions of PVP needed for binding to the nano-sized metal clusters, resulting in stabilization of the nanoclusters. Alkyl and oxygen atom(s) containing substituents, attached to the pyrrolidinone ring, enhance polymer's water solubility and interaction with hydrophobic substrate molecule. The substituent(s) may induce substrate facial recognition, leading to possible selective C-H group oxidation. Previously reported CSPVPs, derived from the polymerization of (*R*)-C5-substituted *N*-vinylpyrrolidinones,[5a] possess a substituent distanced from the C2 carbonyl group of the amide function, needed for complexation to the metal nanoclusters. We therefore investigated two new classes of CSPVPs possessing asymmetric centers at C3 and C4 or C3 alone of the pyrrolidinone ring and examined their effects on the polymer chain stereochemistry, stabilization, and induction of chirality in the bimetallic nanoclusters as well as the effectiveness in catalytic C-H group oxidation. In addition, the availability of both opposite chiral polymers, (−)-**1R** and (+)-**1S** (Scheme 1), allows the examination of match and mismatch in stereochemistry with chiral

Author Manuscript Author Manuscript Author Manuscript Author Manuscript

substrates, which may shed light into the scope and applicability of the systems. A review on gold and gold-based bimetal nanoclusters including characterizations and proposed mechanisms on oxidation reactions has been reported,[5b] but with limited applications.

Catalytic oxidation of non-activated C-H groups remains one of the most challenging transformations in synthetic organic chemistry.[11] Oxidation using enzymes such as P450 oxygenases and homogeneous catalysts were usually explored, since site selectivity and enantioselectivity are often achieved. In the former case, different classes of substrate molecules require the finding of proper oxygenases to affect the oxidation, and in the latter case, ligands in the organometallic or organo-catalysts are not readily available commercially in many cases and may require development of specific catalysts for particular C-H oxygenation reaction.[11] Heterogeneous catalysts are readily prepared in general and can be separated from the products and recovered, hence, they are preferred by the industry.[12] However, heterogeneous catalysts are less specific and often produce side or over oxidized products. Bimetallic nanoclusters are considered heterogeneous catalysts[5] even though they are soluble in water and polar organic solvents such as $CH_3CN$ and DMF. Due to numerous aliphatic C-H bonds in a molecule, a low dissociation-energy bond or a directing group is needed in controlling the regioselectivity of the oxidation.[11d,11i] Previous works reported C-H oxidation of six cycloalkanes using only Cu/Au stabilized by CSPVPs, derived from amino acids, and $H_2O_2$ as an oxidant (Scheme 1, Previous Work).[5a] Herein, the synthesis of second-generation CSPVPs, derived from inexpensive chemicals such as *D*-isoascorbic acid, *D*-ribose, and *L*-malic acid, are described. They were utilized in the stabilization of Cu/Au or Pd/Au bimetallic nanoclusters and oxidation of ten cyclic molecules including cyclic ethers, rigid molecules, and bioactive natural products, using hydrogen peroxide or *t*-butyl hydroperoxide as an oxidant (Scheme 1, This Work). The stereochemistry of the polymer chains were studied by $^{13}C$ NMR spectroscopy, polymer chain lengths by high-resolution mass spectrometry (HRMS), and chiroptical responses of the bimetallic nanoclusters by circular dichroism (CD).

The electronegativity values for Au, Cu, and Pd are 2.54, 1.90, and 2.20, respectively,[13] suggesting the highest electron-positive Au depolarizes or pulls electron from Cu or Pd in the Cu/Au or Pd/Au bimetallic nanoclusters. Consequently, Au induces an enhanced partially and positively charged Cu or Pd atom. This in turn affords a highly electrophilic and reactive Cu or Pd atom suitable for C-H group oxidation.

## RESULTS AND DISCUSSION

### Syntheses of chiral *N*-vinylpyrrolidinones (−)-6, (+)-10, and (−)-13

The availability of both enantiomers (*R*)- and (*S*)-CSPVP would allow the study of chiroptical responses of the encapsulated bimetallic nanoclusters. Hence, enantiomers, *N*-vinylpyrrolidinone (−)-**6** and (+)-**10**, possessing opposite asymmetric centers at C3 and C4 of the pyrrolidinone ring, and (*S*)-**(−)-13**, possessing asymmetric center at C3, were synthesized, and the corresponding chiral polymers were produced *via* free-radical polymerization processes (Schemes 2 and 3). The stereogenic center(s) may provide an "enantiomorphic-site control" effect to generate stereo-regulated polymers in the polymer

Author Manuscript Author Manuscript Author Manuscript Author Manuscript

main chain[14], thereby producing a structurally defined polymer frame work and improving the stereoselectivity of the oxidation reactions.

The required precursors, lactone **4** and azide **5**, were synthesized by modification of a reported procedure,[15] *via* a sequence of reactions (Scheme 2): (i) oxidative cleavage of *D*-isoascorbic acid (**3**)[16] (93% yield); (ii) acetonide formation of the resulting *D*-erythronolactone[17] (lactone **4**; 78% yield); and (iii) ring opening of the lactone with sodium azide[15] (azide **5**; 54% yield). In the sodium azide reaction, lactone **4** was recovered in 32%, which likely derived from the nucleophilic addition of azide ion onto the carbonyl group of **4** followed by ring opening. The resulting acyl azide undergoes ring closure upon aqueous work-up to regenerate lactone **4**. Reduction of the azido function of **5** with hydrogen and Pd/C in methanol (91% yield) followed by sublimation at 150 °C/0.1 mm Hg (97% yield), and *N*-vinylation with 5 mol% of 4,7-diphenyl-1,10-phenanthroline palladium bis(trifluoroacetate) [(DPP)Pd($OCOCF_3$)$_2$][18] and *n*-butyl vinyl ether at 75 °C gave vinyllactam (−)-**6** in an 86% yield. The structure of (−)-**6** was unequivocally characterized by a single-crystal X-ray analysis (Figure 1).

The opposite stereoisomer of lactam (−)-**6**, *N*-vinyllactam (+)-**10**, was produced from lactone (+)-**9**, a known compound, which was conveniently prepared from *D*-(−)-ribose (**8**)[19] by the formation of acetonide (98% yield) followed by reduction and oxidative cleavage (91% yield), and Swern oxidation of the resulting lactol (81% yield) (Scheme 2). Azidation of lactone **9** followed by hydrogenolysis, sublimation, and *N*-vinylation with *n*-butyl vinyl ether and 4.6 mol% of (DPP)Pd($OCOCF_3$)$_2$ furnished (+)-**10** in a 33% overall yield.

The C3 substituted chiral vinyl lactam (−)-**13**, a precursor for the synthesis of chiral polymer (−)-**2**, was prepared from (*S*)-2-(methoxymethoxy)butanolide (**12**), a previously reported molecule,[20] derived from L-(*S*)-malic acid (Scheme 3).[21] Hence, protection of L-malic acid followed by borane reduction, ring closure under acidic medium, and alkylation with chloromethyl methyl ether (MOMCl) afforded lactone (−)-**12** in a 62% overall yield. Following the aforementioned azidation by sodium azide, reduction by hydrogen over palladium/carbon, annulation under sublimation conditions, and vinylation by *n*-butyl vinyl ether, lactone (−)-**12** was converted into (−)-**13** in a 36% overall yield.

## Syntheses and characterization of chiral substituted poly-*N*-vinylpyrrolidinones and bimetallic nanoclusters

Different catalysts and reaction conditions affect the polymer main chain stereochemistry in the polymerization of terminal alkenes.[10b,14,22] However, due to the presence of reactive amide and *N*-vinyl functions, a free-radical process was chosen for the polymerization of *N*-vinyllactams.[10b,22a] The polymerizations of vinyllatams (−)-**6**, (+)-**10**, and (−)-**13** were carried out under thermal condition and photochemical condition. Stereochemistry in the main chain of the resulting polymers was studied. A dispersion polymerization method[23] was adapted by heating (−)-**6**, 1% of copolymer **7** and 0.2 mol% of azobisisobutyronitrile (AIBN) in ethyl acetate in a sealed tube at 70 °C to give polymer (−)-**1R** in a 98% yield (Scheme 2). Copolymer **7** was added to produce a uniformed polymer[23] and was made from

Author Manuscript Author Manuscript Author Manuscript Author Manuscript

**(−)-6** and 1 equiv. of vinyl acetate along with 1 mol% of AIBN in acetone at 70 °C under nitrogen in a sealed tube.

Similarly, using this thermal process, chiral polymers (+)-**1S** and (−)-**2** were synthesized as depicted in Scheme 2 and 3, respectively. Hence, vinyl lactams (+)-**10** and (−)-**13** were separately treated with 1% of the respective copolymer, **11** and **14**, 0.2 mol% of AIBN in ethyl acetate under thermal condition (70 °C) to give (+)-**1S** and (−)-**2**, respectively. Photo-polymerization reactions were also carried out by treating vinyl lactams (−)-**6**, (+)-**10**, and (−)-**13** separately with 1% (by weight) of the corresponding copolymer **7**, **11**, and **14**, and 0.2 mol% of AIBN in ethyl acetate under UV light irradiation at 0 °C in a sealed tube. Polymers (−)-**1R**, (+)-**1S**, and (−)-**2** were respectively obtained in 83 – 88% yields (Schemes 2 and 3). Molecular weights and specific rotations of the synthesized CSPVPs were determined and data summarized in Table 1.

The molecular weights of polymers can be determined by several methods including NMR, gel permeation chromatography (GPC), and mass spectrometry. The NMR method is based on comparison of integrals of the end group and the repeating unit. However, the end-group signal (2-cyano-2-propyl group) is overlapping with the up-field region of the polymer signal in polymers (−)-**1R**, (+)-**1S**, and (−)-**2**, excluding this application. Attempts to apply GPC/HPLC, equipped with an ELSD-LTII (evaporative light-scattering) detector along with UV and RI detectors, and using different size-exclusion chromatographic columns, including a combination of TSKgel α−400 and TSKgel α-M (from Tosoh Bioscience), to study the molecular weights of CSPVPs with PVPs as standards, failed. GPC retention times of different sizes of PVP are not in agreement with those of CSPVPs. Likely, the structural differences in PVP and CSPVP affect their solubility in various solvents, leading to different retention times in the GPC studies. The number average molecular weight ($M_n$) and weight average molecular weight ($M_w$) of chiral polymers were therefore determined by high-resolution mass spectrometry (HRMS)[24a] using a Quadrupole Time-of-Flight (QTOF) mass spectrometer, and results are depicted in Table 1. Method for obtaining the molecular weights described in Supporting Information 2 (SI2). Polymers (−)-**1R** and (+)-**1S**, derived from thermal reactions, showed respective weight average molecular weight, $M_w$, of 89,051.471 (number of monomer units, n = ~486) and 80,021.8097 Da (n = ~437), and specific rotation of $[\alpha]_D^{22}$ = −42.7 (c 0.5, $CHCl_3$) and $[\alpha]_D^{22}$ = +35.3 (c 0.5, $CHCl_3$), suggesting the polymerization processes gave similar lengths of chiral polymers.

Polymers that derived from photochemical reactions, (−)-**1R** and (+)-**1S**, have lower molecular weights, $M_w$ of 53,547.9798 (n = ~292) and 48,459.1355 (n = ~283), and smaller specific rotations, −38.0 and +32.4, comparing with those obtained from thermochemical reactions (Table 1). Similarly, the molecular weight and specific rotation of (−)-**2** obtained from the thermochemical reaction are greater than those from photochemical reaction. The differences in magnitudes of specific rotations may derive from the differences in polymer lengths, hence the longer polymer has a larger specific rotation value. The polydispersity index, PI values ($M_w/M_n$) of (−)-**1R**, (+)-**1S**, and (−)-**2** obtained from thermochemical reactions are 1.04 – 1.07, revealing the polymers are uniform in sizes. Similar PI values, 1.03 – 1.08, were found from polymers obtained from photochemical reactions. To evaluate whether different polymer lengths would affect the stability of the nanoclusters, different

Author Manuscript Author Manuscript Author Manuscript Author Manuscript

lengths of CSPVP and PVP were synthesized by varying the amounts of AIBN in the free-radical polymerization reactions. Table 2 summarized $M_n$, $M_w$ and intrinsic viscosity values of different lengths of (−)-**1R**, (+)-**1S**, and (−)-**2** along with synthesized PVPs from polymerization reactions. Results indicated that greater the amounts of AIBN, shorter the polymer lengths, which is in agreement with the free-radical polymerization mechanism. Various Cu/Au (3:1) and Pd/Au (3:1) bimetallic nanoclusters were prepared (Scheme 3) in aqueous solution using different sizes of CSPVP, and their stabilities were studied by prolong standing at elevated temperatures. Bimetallic nanoclusters obtained from chiral polymers, preparing from 0.2 mol% AIBN, showed the greatest stability. CSPVPs having shorter polymer length ($M_w$ < 30,000) gave less stable bimetallic nanoclusters, which decomposed at 25 °C in 24 hours, while CSPVPs possessing longer polymer length ($M_w$ > 100,000) have low solubility in water, resulting in a poor yield of nanoclusters. This was indicated by the metallic metal precipitation during the preparation process. The relative sizes of a same class of polymers can be determined by measuring the intrinsic viscosity, [η], of the polymers. The viscosity of a molecule is generated from the intermolecular attractive force, hence the larger the polymer, the greater is its viscosity value.[24b] Using an Ubbelohde viscometer, intrinsic viscosity of chiral polymers (−)-**1R**, (+)-**1S**, and (−)-**2**, and three synthetic PVPs were measured in methanol and results are summarized in Table 2. Methods for measurement and determination of [η] are described in SI2. Results of intrinsic viscosities shown in Table 2 correlate well with the molecular weights found from HRMS, in that a larger polymer shows a greater viscosity value. However, the intrinsic viscosity values of CSPVPs can not be used to correlate with those of PVPs. Likely, the intermolecular interaction of CSPVP in methanol is different from that of PVP. Plots of intrinsic viscosities vs molecular weights (from HRMS) of different sizes of CSPVPs and PVPs separately showed linear correlations (see SI2, Figure SI2–5).

The synthesized polymers are soluble in water and organic solvents including dichloromethane, acetonitrile, and methanol, and are insoluble in non-polar solvents such as hexane. They are used in the catalytic oxidation reactions and can be recovered after the reactions [see Supporting Information 1 (SI1) Experimental Section or ES].

In addition to the measurements of specific rotation, molecular weight and intrinsic viscosity of CSPVP, circular dichroism (CD) and $^{13}C$ NMR spectroscopy were carried out for characterization of their macromolecular structure and backbone stereochemistry. CD spectra of (−)-**1R**, (+)-**1S**, and (−)-**2** were recorded at 3 μM concentration in water and displayed in SI1, Figure SI1–1. A strong absorption band was found for (−)-**1R** possessing a negative molar ellipticity [θ] value of −201 mdeg at λ = 223 nm, and (+)-**1S** a positive molar ellipticity value of +180 mdeg at λ = 219 nm (SI1, Figure SI1–1, left panel, overlay spectra). No other absorptions observed after 230 nm, and the two absorption graphs are symmetric, revealing two opposite conformational handiness. Chiral polymer (−)-**2**, like (−)-**1R**, showed a strong negative absorption band at 221 nm with [θ] value of −92 mdeg. There are no differences in the CD spectra of those obtained from thermal and photochemical reactions (graphs not shown). Notably, these CD spectra are very different from those of bimetallic nanoclusters stabilized by chiral polymers (*vide infra*).

Author Manuscript Author Manuscript Author Manuscript Author Manuscript

Carbon-13 NMR spectroscopy has been used to study the tacticity of poly(vinylpyrrolidinone) (PVP) polymer chain,[22a,22b,24b] hence, it was applied to gain information of the chiral polymer chain stereochemistry, in which the polymers were derived from both thermal and photochemical reactions. $^{13}C$ NMR spectra were recorded at 100 MHz in $CDCl_3$ and representative spectra of (+)-**1S** and (−)-**2**, obtained from both thermal and photochemical reactions, are shown in SI1, Figures SI1–2A – 2D. The spectra of (+)-**1S** and (−)-**1R** are identical (see SI2). The $^{13}C$ spectra were also recorded at 150 MHz in $CDCl_3$ or $D_2O$ (see SI2), but no significant changes in signal appearances were found. The broad signals at δ 44.7 – 47.0 ppm and 43.0 – 44.5 ppm in the zoom-in spectrum of (+)-**1S** are assigned[22b,22d] for α-CHN and $CH_2N$, respectively (SI1, Figures SI1–2E and –2F). Similarly, signals at δ 43.3 – 46.0 ppm and 37.7 – 40.0 ppm in the spectrum of (−)-**2** are respectively assigned for α-CHN and $CH_2N$ (SI1, Figures SI1–2G and –2H). The α-CHN and $CH_2N$ signals of (+)-**1S** are unresolved, hence it is not possible to assign the polymer main chain tacticity. However, the α-CHN signals at δ 43.3 – 46.0 ppm region of (−)-**2**, showing three signals at δ 45.3, 44.1, and 43.6 ppm. They are assigned to the triad stereo-sequences of mm + mr, rr, and mr (mm is isotactic, rr is syndiotactic, and mr is heterotactic triad). The assignments are assumed based on those reported α-CHN chemical shifts and tacticity assignment in PVP.[22d] The peak intensities can not be used for quantitative determination of the triad tacticities, since the mm and mr contributions in the δ 45.3 ppm signal are unknown.[22b] Based on the spectra, isotactic, syndiotactic and heterotactic triads are likely present as block polymer, in polymer (−)-**2** as well as (−)-**1R**.

Gold was used in bimetallic nanoclusters due to its synergistic electronic effects[25] and enhancement of the reactivity of Cu or Pd (*vide supra*). Different ratios of Cu/Au and Pd/Au, such as 1:1, 2:1 and 3:1, were investigated, and a 3:1 ratio provided the highest reactivity. A co-reduction of mixed ions method[5a,25,26] was utilized for the preparation of Cu/Au (3:1) or Pd/Au (3:1) stabilized by CSPVP or PVP (40K MW). For example, a solution of (−)-Cu/Au (3:1)/**1R** was prepared by the treatment of $HAuCl_4$ (1 equiv.), CuCl (3 equiv.) and (−)-**1R** (0.11 equiv.; based on the moles of Au) in deionized and degassed water with $NaBH_4$ at 25 °C for 2 h (see SI1) to give a clear-dark-purple colloidal dispersion of bimetallic nanocluster solution (Scheme 3). Similarly, $Na_2PdCl_4$ (3 equiv.), $HAuCl_4$ (1 equiv.), CSPVP (−)-**1R** (0.11 equiv.) and $NaBH_4$ were used to prepared (−)-Pd/Au (3:1)/**1R**, resulting in a clear purple-brown solution (SI1). The bimetallic nanocluster solutions are stable at 25 °C and used in the catalytic C-H group oxidation reactions without further manipulation. Different concentrations of the bimetallic nanoclusters were obtained by using either less or more water. Bimetallic nanocluster concentrations ranging from 10 to 25 mM were prepared, and a higher the concentration, a greater the relative reaction rate. For characterization purpose, the aforementioned bimetallic nanocluster solution was filtered through a Vivaspin 20 centrifugal filter device (3,000 MWCO), and washed with deionized water twice to remove low molecular weight inorganic materials. The resulting nanoclusters were dissolved in water and subjected to various analyses including transition electron microscopy (TEM), atomic force microscopy (AFM), dynamic light scattering (DLS), CD, UV, inductively coupled plasma-mass spectroscopy (ICP-MS), NMR, and IR (see SI2).

Author Manuscript Author Manuscript Author Manuscript Author Manuscript

Cu/Au- (3:1) or Pd/Au- (3:1) CSPVP solution was dissolved in 1% $HNO_3$/2% HCl solution and subjected to the ICP mass spectrometer. Standard solutions for $^{197}Au$, $^{106}Pd$ and $^{65}Cu$ (1000 ppm of metal in 30 mL of water) were used and results of Cu/Au (3:1)-**1R** and Pd/Au (3:1)-**1R** showed concentrations of Cu/Au and Pd/Au are 3:1, confirming the metal compositions in the bimetallic nanoclusters. The average sizes, size distribution, and shapes of polymers (−)-**1R**, (+)-**1S** and (−)-**2** were measured by AFM and DLS (see SI2). For instance, chiral polymer (−)-**1R** showed in DLS an average size of ~14.6 nm with narrow distribution (11.4 – 18.2 nm) and in AFM sizes of ~15 – 30 nm, showing structurally undefined shape. TEM revealed the average sizes of (−)-Pd/Au (3:1)-**1R** and (−)-Cu/Au (3:1)-**1R** nanoclusters being 3.32 ± 1.08 and 3.41 ± 1.13 nm, respectively. The amide C=O absorption band of the pyrrolidinone ring at 1648 $cm^{-1}$ of polymer (−)-**1R** in IR spectrum shifted to 1642 $cm^{-1}$ in (−)-Pd/Au (3:1)-**1R** and 1643 $cm^{-1}$ in (−)-Cu/Au-**1R**, suggesting a greater character of $^{\delta-}O\text{-}C{=}N^{\delta+}$ of the amide group in the nanoclusters than that of (−)-**1R**, due to chelation with the metals. Under similar reaction conditions, in the absence of CSPVP such as (−)-**1R** or PVP, reduction of $Na_2PdCl_4$, $HAuCl_4$ with $NaBH_4$ gave insoluble black solids, i.e., no nanoclusters were formed.

The chirality of nanoclusters may contribute by chirality of the ligand, e.g., glutathione in bimetallic nanoclusters,[27a] or chiral polymer, e.g., chiral poly(fluorine-alt-benzothiadiazole) in gold nanoparticles.[27b] This may be due to the formation of chirally ordered nanocomposite.[27b] We were intrigued whether the chirality of CSPVP can induce chiroptical responses in our bimetallic nanoclusters, which may shed light on optically active nanomaterials and their catalytic reactions. Indeed, CD spectra of bimetallic nanoclusters encapsulated by CSPVPs displayed characteristic absorptions in their CD spectra (Figure 2). Cu/Au (3:1)-**1R** spectrum at 1.5 mM concentration showed distinctive strong negative absorptions at 238 nm (−31 mdeg) and 215 nm (−33 mdeg), and positive absorptions at 253 nm (+38 mdeg) and 230 nm (+22 mdeg). On the other hand, Cu/Au (3:1)-**1S** spectrum showed positive absorptions at 237 nm (+79 mdeg) and 213 nm (+33 mdeg), and negative absorptions at 251 nm (−27 mdget) and 228 nm (−21 mdeg) (see SI2). An overlay of these two spectra is shown in Figure 2, left panel, revealing Cu/Au made from (−)-**1R** and (+)-**1S** displayed nearly mirror-imaged CD spectra, despite small differences in their wavelengths and magnitudes of the Cotton effects. These minor changes may be due to the different lengths of chiral polymers, **1R** and **1S**, and changes in Cotton effects are caused by conformer populations.

Similarly, an overlay of spectra of Pd/Au (3:1)-**1R** and Pd/Au (3:1)-**1S** presented in Figure 2, right panel, showing opposite CD spectra. The CD spectrum of Cu/Au (3:1)-**2** at 1.5 mM in water is shown in SI1 Figure SI1–3 and a strong negative absorption appeared at 236 nm (−56 mdeg). Notably, the CD spectrum of (−)-**1R** or (+)-**1S** (see SI1, Figure SI1–1, left panel) at 3 μM concentration exhibited a strong and single negative or positive absorption at ~220 nm, respectively, suggesting the aforementioned bimetallic nanoclusters' chiroptical responses are contributed from chiral-polymer encapsulated nanomaterials and not from the chiral polymer alone. The nanoclusters likely possess defined and discrete chiral polymer structures and possibly chiral arrangement of the metal atoms. The CD spectra of Au, Pd, and Cu alone as controls, showed no absorption (see SI2, Figure SI2–9).

Author Manuscript Author Manuscript Author Manuscript Author Manuscript

## Catalytic C-H bond oxidation of complex natural products and rigid cyclic molecules

The diverse catalytic oxidations of copper-containing oxidases[28a,b] such as dicopper particulate monooxygenase,[28c] have in part motivated numerous studies in C-H functionalization[28d,e] due to copper's oxidative efficiency.

The use of bimetallic nanoclusters Cu/Au (3:1)-$H_2O_2$ or Pd/Au (3:1)-*t*-BuOOH in the C-H group oxidation of cyclic ethers, rigid molecules, heterocycles, and fused aromatic cycloalkanes has not been reported previously.[5a] Hence, (−)-ambroxide (**15**), *R*-(+)-menthofuran (**18**), (+)-2,9-di-(*O*-pivalyl)-boldine *N*-oxide (**23**), 1-adamantanol (**28**), *N*-acetylamantadine (**31**), and *N*-acetylmemantine (**33**) (Scheme 4) as well as (+)-3-pivaloyl estrone (**36**), (+)-*N*-acetyl-dehydroabietylamine (**41**), and (−)-9-allogibberic acid (**46**) (Scheme 5) were chosen for studies.

The oxidation of **15**, a cyclic ether natural product, was carried out first to examine the catalytic activity and regioselectivity of monometallic and bimetallic nanocluster catalysts, Cu/Au (3:1) and Pd/Au (3:1) stabilized by PVP (40 K) or CSPVP (10 mM concentration each in water), using 2 equiv. 30% hydrogen peroxide as an oxidant. At room temperature, there was no reaction, however, the reaction proceeded gradually upon heating. Results of the oxidation reactions summarized in Table 3 and Scheme 4, revealing distinctive matched and mismatched chiral bimetallic-nanocluster catalysts with the chiral substrate, **15**. In the absence of nanocluster catalysts, no oxidized product was found at 80 °C for 3 days and only starting material **15** was recovered (Table 3, Entry 1). Monometallic nanoclusters, 5 mol%, such as Au-PVP, Cu-PVP, and Pd-PVP, were also applied (Entries 2 – 4), and no oxidized product was detected, except in the case of Pd-PVP, where trace amounts of sclaral (**16**) and (+)-sclareolide (**17**) were isolated (Entry 4). The oxidation of **15** proceeded when 5 mol% of Pd/Au (3:1)-PVP or Cu/Au (3:1)-PVP were used (Entries 5 and 6), albeit only 28% and 33% conversion, respectively. However, when Cu/Au-**1R** was applied, 37% yield of **17** was isolated along with 51% recovery of **15** (Entry 7). Strikingly, Cu/Au-**1S** and Cu/Au-**2** produced merely 1% and 2% of **17**, respectively, along with 83 – 84% of recovered **15** (Entries 8 and 9).

Results suggest that nanoclusters derived from **1R** polymer matches the stereochemistry of **15**, while those derived from chiral polymers **1S** and **2** mismatches the stereochemistry of **15**. The diastereoselective oxidation of **15** by Cu/Au/**1R** but not Cu/Au-**1S** or Cu/Au-**2** suggests the bimetallic nanoclusters are chiral, and CD studies of nanoclusters (*vide supra*) are in agreement with the finding. The conversion of **15** to **17** can be improved by using 5 mol% of Cu/Au-**1R** (25 mM) in $H_2O$ solution and 40 equiv. of 30% $H_2O_2$. The yield of **17** increased to 64% with a 23% recovery of **15** (Table 3, Entry 10 and Scheme 4). The regioselective oxidation of α-C-H bond of cyclic ether function may be due to its lower bond dissociation energy, ~95 kcal/mol, than other C-H bonds in the molecule. Sclaral (**16**) consisted of an inseparable 2.3:1 ratio of α and β stereoisomers.[29] Treatment of **16** with 1 mol% Cu/Au-PVP and 2 equiv. of 30% $H_2O_2$ at 80 °C for 2 h gave **17** in a 93% yield, suggesting **16** forms first, which undergoes alcohol oxidation to give **17** under the reaction conditions. Oxidations of **15** to **17** using benzil and oxygen under photoirradiation,[30a] tetrabutylammonium decatungstate photocatalyst,[30b] and chiral and achiral organometallic

Author Manuscript Author Manuscript Author Manuscript Author Manuscript

reagents[11c,30c] have been reported previously. Since bimetallic nanoclusters derived from chiral polymers **1S** and **2** provided similar results in the oxidation reactions, in the following studies, results from **1R** and **1S** were presented, but not **2**.

The recognition of medium-size cyclic ether molecules by the bimetallic-nanocluster system led us to study oxidation of a smaller natural product, *R*-(+)-menthofuran (**18**). Delightedly, **18** underwent oxidation with 1 mol% Pd/Au-PVP (10 mM concentration in water) and 2 equiv. of 30% $H_2O_2$ at 25 °C for 7 h to give a 15% yield of (−)-mintlactone (**19**)[31a,b] and 29% yield of (−)-hydroxymintlactone (**20**)[31c] along with 30% recovery of **18** (Scheme 4). Prolong the reaction time did not significantly improve the yield, but produced other unidentifiable over-oxidized by-products. Catalysts Pd/Au-**1R** and Pd/Au-**1S** were also used to examine their reactivity. To decrease the rate of reactions, 0.1 mol% of the catalysts were used, and results are summarized in Scheme 4. In the reaction using **1R**, 13% yield of **19** and 10% yield of **20** along with 35% recovery of **18** were found. When **1S** was used, the yields and recovery were lower than those from **1R**; i.e., 16% and 3% yield of **19** and **20**, respectively, along with 8% recovery of **18**. Hence, a match-and-mismatch in stereochemical outcome is not as apparent comparing with result from **15**, this may be due to the active site, at C2 of **18**, is away from the C6-stereogenic center. Previously, oxidations of **18** were limited to chromic acid,[32] singlet oxygen[33] or cytochromes P450 enzymes[34] and in most cases ring opening products were obtained.[33,34]

The formation of both **19** and **20** from the oxidation of **18** have not been reported prior to this work. In the absence of the bimetallic-nanocluster catalyst, under similar reaction conditions, no product was found and only **18** recovered. The reaction pathways may involve addition of O=$Pd^{II}$/Au-**1R** onto C2,3-double bond, 1,3-allylic migration of (HO)$Pd^{I}$/Au-**1R** from C3 to C7a, followed by oxidation of C2-lactol to lactone. The C7a-Pd(OH)/Au species may either undergoes protonation by $H_2O$ to give **19** or oxidation to give **20**. The facile oxidation of **18** may provide a new pathway for converting substituted furans and pyrroles to the corresponding lactones and lactams.

(*S*)-(+)-Boldine (**21**), an isoquinoline alkaloid, isolated from leaves, stem bark, and roots of *Laurus nobilis* or bay laurel evergreen tree.[35] It possesses antioxidant, anti-inflammatory, and osteoporosis suppressive properties.[36] Oxidation of boldine with various oxidants, such as $H_2O_2$,[37] provided boldine *N*-oxide. C-H oxidation of boldine, its *O*-protected analogs, or its *N*-oxide has not been reported previously. Treatment of **22**, derived from (+)-boldine (**21**) and pivaloyl chloride, with 3 mol% Cu/Au-PVP at 50 °C or Pd/Au-PVP at 50 or 80 °C and 2 equiv. of 30% $H_2O_2$ for 30 h resulted in 98% and 93% recovery of **22**, respectively. No oxidation products, including *N*-oxide **23**, were found from these reactions. Generally, tertiary amine can be oxidized by $H_2O_2$ to give the corresponding *N*-oxide. However, under our oxidation reaction conditions, hydrogen peroxide likely deactivated by bimetallic nanoclusters, resulting in a significant decrease of the oxidation rate of tertiary amine. Hence, we investigated the oxidation of boldine *N*-oxide **23**, generated from the oxidation of **22** with *m*-chloroperbenzoic acid (MCPBA). To our delight, under similar reaction conditions, treatment of **23** with 1 mol% Cu/Au-PVP and 2 equiv. of 30% $H_2O_2$ at 50 °C gave a 9% yield **24**, 4% yield of **25**, 55% yield of **22**, and unidentifiable materials.

Author Manuscript Author Manuscript Author Manuscript Author Manuscript

When 1 mol% of Pd/Au-PVP catalyst was used, **24** (4% yield), **26** (6% yield), and **22** (44% yield) were obtained. The structures were assigned based on their $^{1}$H NMR, $^{13}$C NMR, 2D NOESY (Nuclear Overhauser Effect Spectroscopy), and mass spectra. In brief, $^{1}$H NMR spectrum of compound **24** shows four singlets assigned for three aromatic hydrogens, C3-H, C8-H and C11-H along with an enol OH at δ 6.67 ppm. The C4 and C5 methylene hydrogens appear as two triplets at δ 3.37 (two protons) and 3.27 ppm (two protons), which couple with each other. The two methoxy's, *N*-methyl, and two *t*-butyl groups display five singlets at δ 3.97, 3.84, 3.06, 1.50, and 1.45 ppm, respectively. $^{13}$C NMR and mass spectra are in agreement with the assigned structure (see SI2).

$^{1}$H NMR spectrum of **25** shows four aromatic hydrogens as singlets at δ 9.10, 8.43, 7.62, and 7.58 ppm, and five singlets at δ 4.05, 4.02, 3.88, 1.52, and 1.47 ppm assigned for two methoxys, *N*-methyl, and two *t*-butyl groups, respectively. Similarly, $^{13}$C NMR and mass spectra are in agreement with the assigned structure (see SI2). The $^{13}$C NMR chemical shifts for the two C=O signals at C5 (δ 157.4 ppm) and C7 (δ 176.7 ppm) are in agreement with those reported for C=O of isoquinolones[38] and dibenzo[de,g]quinolin-7-ones.[39] $^{1}$H NMR spectrum of compound **26** reveals five aromatic signals at δ 9.19 (singlet), 8.87 (doublet), 8.13 (singlet), 7.76 (doublet), and 7.57 ppm (singlet) for C8-H, C4-H, C11-H, C5-H, and C3-H, respectively. In addition, four singlets at 4.03, 3.92, 1.51, and 1.46 ppm are assigned for two methoxy and two *t*-butyl groups, and absence of the *N*-methyl signal. $^{13}$C NMR and mass spectra are in agreement with the assigned structure. Notably, oxidation of boldine and its derivatives has not been reported previously. Presumably, the oxy-anion of *N*-oxide binds to bimetallic nanoclusters Cu/Au or Pd/Au and subsequently undergoes intramolecular C-H oxidation at β carbon C7 and α carbon C5, utilizing the oxygen of *N*-oxide. The resulting C7 hydroxyl group oxidizes to give ketone, which enolizes to form aromatic phenanthrenol **24**. On the other hand, the C5 hydroxyl group of **23** oxidizes to give amide, which proceeds oxidative dehydrogenation followed by C-H oxidation at C7 to furnish **25**. Dibenzo[*de,g*]quinolin-7-one **26** may derive from demethylation of **23** followed by oxidative aromatization of the piperidine ring and C-H bond oxidation at C7. Demethylation of dialkylmethylamine *N*-oxides has been reported under reductive conditions by using sulfur dioxide[40] or ferrous sulfate[37] *via* a rearrangement mechanism,[40] while demethylation under oxidative conditions has not been utilized previously. The *N*-oxide directed intramolecular oxidation and demethylation of *N*-methylamine *N*-oxide reactions are unprecedented. Molecule **23** is chiral, possessing C6a-*S* configuration, while oxidized products **24** – **26** are achiral, hence, oxidation of **23** with Cu-Au-**1R** or −**1S** under these conditions was not investigated.

In support of the assumption that the oxy-anion of *N*-oxide binds to bimetallic nanoclusters Pd/Au followed by C-H oxidations at β-C7 or α-C5 carbons, *N*-oxide **23** was treated with 5 mol% of Pd/Au-PVP in acetonitrile and water without an oxidant such as $H_2O_2$. Expectedly, deoxygenated amine **22** (15% yield), C7-oxidized product **24** (11% yield), and a new molecule, **27** (13% yield) along with recovered **23** (54%) were isolated and characterized. Results suggest that the *N*-oxide group is the oxygen source for C-H oxidation either intramolecularly and/or intermolecularly. The lesser amount of amine **22** than the total amounts of **24** and **27** implies that intramolecular delivery of the oxygen atom is likely. The

Author Manuscript Author Manuscript Author Manuscript Author Manuscript

structure of compound **27** was characterized based on its $^{1}H$, $^{13}C$, and 2D NOESY NMR, and MS spectra. In the 2D NOESY spectrum, correlations were found between C5H at δ 7.83 ppm and C6a and C7 at δ 3.33 and 3.22 ppm, between C8H at δ 7.19 ppm and C7 and C6a, and between C3H at δ 7.54 ppm and C4H at δ 7.68. A proposed mechanism for the formation of **27** and **22** from **23** is depicted in Scheme 6 (*vide infra*). The presence of $H_2O_2$ in the oxidation of **23** appears to promote the deoxygenation of *N*-oxide function of **23**, leading to amine **22**. It was anticipated that *N*-oxide molecules such as *N*-methylmorpholine *N*-oxide (NMO) may serve as a suitable oxidant in this case and DMF can be used as a solvent for the preparation of bimetallic nanoclusters and oxidation reaction.

It is noteworthy that compound **23** and the aforementioned oxidized products have low solubility in water and acetonitrile. The use of DMF as a solvent would allow the reaction to be conducted at high concentrations, leading to an increase of reaction rate. Hence, **23** was treated with 0.3 mol% of Pd/Au-PVP (25 mM in DMF) and 2 equiv. of NMO in DMF, providing a final concentration of 0.89 M. To our amazement, the reaction took place at 25 °C for 16 h to give a 52% yield of **27** and 26% recovery of **23**. Compound **22** was not found. As mentioned above, **27** likely forms from **23,** and in this case NMO binds to Pd/Au resulting in *N*-methylmorpholine-Pd(=O)/Au, which undergoes C5-H bond oxidation of Pd/Au-bound **22**, derived from **23**, or oxidation of the amine function of **22** to give **23**. The use of 0.3 mol% of Pd/Au-**1R** or Pd/Au-**1S** gave similar results as those using 0.3 mol% Pd/Au-PVP, albeit in a decrease of relative reaction rates (Scheme 4). Compound **23** possesses a planar structure, which likely does not result in a facial selectivity by Pd/Au-**1R** or Pd/Au-**1S**. An increase of the amount of catalyst to 1.3 mol% Pd/Au-PVP, under similar reaction conditions, afforded a 63% yield of **27**. A reduction of the oxidant to 1 equiv. of NMO provided a 55% yield of **27** and 8% of recovered **23**. The reaction illustrates an unprecedented one-pot oxidation-elimination of boldine *N*-oxide derivative **23** to give a good yield of **27** as the sole product.

Rigid molecules such as 1-adamantanol (**28**), *N*-acetylated amantadine [or 1-(*N*-acetylamino)-adamantane] (**31**) and *N*-acetyl-memantine [or 1-(*N*-acetyl)-amino-3,5-dimethyladamantane] (**33**) were investigated next to probe the relative reactivity of their tertiary, secondary and primary C-H bonds. Treatment of 1-adamantanol (**28**) with 5 mol% of Cu/Au-PVP (10 mM aqueous solution) and 2 equiv. of 30% $H_2O_2$ in acetonitrile (the final concentration of the reaction solution is 0.03 M) at 25 °C for 24 h gave a 27% yield of 1,3-adamantanediol (**29**) and 5% yield of $1,4_{eq}$-adamantanediol (**30**) along with a 49% recovery of **28**. The use of 5 mol% Cu/Au-CSPVP **1S** under similar reaction conditions gave similar results, 30% yield of **29** and 7% yield of **30** along with 41% recovery of **28**. Both **29** and **30** are meso compounds, and oxidation of **28** using Cu/Au-CSPVP **1R** provided similar results (Scheme 4). An increase of the oxidant $H_2O_2$ from 2 equiv. to 15 equiv. under similar reaction conditions afforded 39% and 20% yield of **29** and **30**, respectively, along with a 11% of recovered **28**. **The spectral data of 29**[41] and **30**[42] are in agreement with those reported.

Amantadine is used for influenza A and Parkinsonian syndromes,[43] while memantine for moderate-to-severe Alzheimer's disease.[44] Both amantadine and memantine antagonize *N*-

Author Manuscript Author Manuscript Author Manuscript Author Manuscript

methyl-*D*-aspartate receptor (NMDAR), and they possess various side effects.[45] Hence, analogs with lesser side effects and enhanced efficacy are preferable. C-H group oxidation of these molecules may lead to new analogs for biological studies. *N*-Acetyl-amantadine (**31**) underwent oxidation by the treatment with 5 mol% Cu/Au (3:1)-PVP and 20 equiv. of 30% $H_2O_2$ in acetonitrile-$H_2O$ at 80 °C for 3 days to give **32**, a meso molecule, in 35% yield along with 48% recovery of **31**. An increase of the temperature to 90 °C, under similar reaction conditions a 51% yield of **32** and 19% recovery of **31** were isolated. The spectral data of **32** is in agreement with those reported.[42] The oxidation took place at the tertiary carbon of **31**, which may due to a weaker tertiary C-H bond energy (96.5 kcal/mol) comparing with the secondary C-H bond energy (98.5 kcal/mol).

Interestingly, when *N*-acetylmemantine (**33**) was treated with 1.3 mol% Cu/Au (3:1)-**1R** and 3 equiv. of 30% $H_2O_2$ at 80 °C for 30 h, respective tertiary and secondary C-H oxidation products, **34** (23% yield) and equatorial hydroxyl **35** (4% yield), were isolated along with 60% recovery of **33**. The use of 1.3 mol% Cu/Au-PVP provided similar results, 22% yield of **34**, 6% yield of **35** and 50% recovery of **33**. On the other hand, the oxidation reaction using 1.3 mol% of Pd/Au-PVP is sluggish and gave only 8.3% yield of **34** and 1% yield of **35** as well as 83% recovery of **33**. The structure of **34** was characterized by its NMR spectra, which are identical to those reported,[11c] while that of **35** was identified through a single-crystal X-ray analysis (Figure 3). To our delight, similar to the oxidation of **28**, an increase of oxidant from 3 equiv. to 20 equiv. of 30% $H_2O_2$ at 50 °C for 3 days, 38% and 17% yield of **34** and **35**, respectively, were isolated along with 12% of recovered **33**. Hence, an increase of the amount of oxidant facilitated the rate of oxidation reactions and chemical yields. The methylene C-H oxidation of **33** leading to **35**, a previously unreported molecule, is unusual. It can be converted into novel analogs for the discovery of Alzheimer drug.[44,45]

The captivating results obtained from the oxidation of boldine derivative **23** led us to investigate oxidations of other bioactive natural products containing aromatic ring (Scheme 5). 3-*O*-Pivaloyl estrone (**36**) was prepared in an 89% yield by the esterification of estrone with pivaloyl chloride and pyridine. Attempted oxidation of **36** with 5 mol% Cu/Au (3:1)-**1R** or -PVP and an oxidant, 30% $H_2O_2$ (2 equiv.) in acetonitrile-water at 70 °C for 3 days failed to provide oxidized products. Similarly, 5 mol% Pd/Au-PVP and 2 equiv. of 30% $H_2O_2$ did not produce appreciable products. However, when *t*-BuOOH, a stronger oxidant than $H_2O_2$, was applied, satisfactory results were found. Hence, treatment of **36** with 1 mol% Pd/Au-**1R** and 1.5 equiv. of *t*-BuOOH in acetonitrile-$H_2O$ at 70 °C gave 9,11-dehydro-3-pivaloyl-estrone (**37**) (20% yield), 6-oxo-3-pivaloyl-estrone (**38**) (20% yield), 9-hydroxy-6-oxo-3-pivaloyl-estrone (**39**) (9.5% yield) and 9,11-dehydro-6-oxo-3-pivaloyl-estrone (**40**) (2% yield) along with 33% of recovery of **36** (Scheme 5). Spectral data of **38** and **39** are identical with those reported.[46] Hence, *t*-BuOOH appears to be more effective for benzylic oxidation reactions than hydrogen peroxide. The oxidation of **36** with 1 mol% Pd/Au-PVP and *t*-BuOOH produced **37** – **39**, under similar reaction conditions, but in lower chemical yields (Scheme 5). The reaction of **36** with Pd/Au-CSPVP **1S** and *t*-BuOOH showed a similar relative reaction rate as that of PVP, suggesting the match and mismatch in stereochemistry is not significant. This may be due to that estrone molecule is relatively flat and the small hydrogens at C8 and C9 do not offer a strong facial discrimination.

Author Manuscript Author Manuscript Author Manuscript Author Manuscript

Oxidation of (+)-**36** with 1 mol% of Cu/Au-PVP (25 mM concentration) and 1.5 equiv. of *t*-BuOOH at 70 °C afforded 20% and 18% yield of **38** and **39**, respectively. Increasing the amounts of catalyst and oxidant improved the chemical yield and lowered the reaction temperature and time. Thus, oxidation of **36** with 3 mol% of Cu/Au-PVP and 4 equiv. of *t*-BuOOH at 50 °C for 18 h, **38** and **39** were isolated in 45% and 24%, respectively, along with 5% of recovered **36**. Cu/Au-**1R** gave similar results. Dehydroestrone **37** and starting estrone **36** are inseparable and they were deacylated with $K_2CO_3$ in methanol to give the corresponding phenols, which were separated by silica gel column chromatography. Spectral data of the resulting 9,11-dehydro-estrone is identical to that reported.[47] Presumably, **36** undergoes benzylic oxidation to give 9-hydroxy- and 6-hydroxy-3-pivaloyl estrones. The former undergoes β-elimination to give **37** and the latter undergoes oxidation to give **38**. Product **39** likely derived from the double oxidations at C6 and C9 followed by oxidation of the C6 hydroxyl group and dehydration of the C9-OH and C11-H. Compound **40** would derive from the dehydration of **39** *via* a β-elimination. The structure of **40** was assigned based on $^1$H, $^{13}$C, 2D COSY and 2D NOESY NMR (see SI2) and mass spectra. In the 2D NOESY spectrum, correlations were found between C1-H signals at δ 7.25 ppm and C11-H at 6.50 ppm, establishing C9,11-double bond assignment. $^{13}$C NMR spectrum showed carbonyl groups of C6 at δ 196.2 ppm and C17 at δ 220.0 ppm. The selective benzylic C-H oxidation may be attributed to a weak bond-dissociation energy of the benzylic C-H bond, ~90 kcal/mol. Results reveal a similar rate of oxidations at benzylic C6 and C9 C-H bonds accompanying by a rapid oxidation of the resulting secondary hydroxyl group.

The aromatic abietane diterpenoids have shown diverse bio-activities,[48] and benzylic oxidation at C7 of *N*-acetyl-dehydroabietylamine (**41**) with chromic anhydride led to various analogs with anti-leishmanial activity.[49] Catalysts such as bimetallic nanoclusters Pd/Au or Cu/Au would be good candidates for replacing chromic anhydride, a toxic chemical. Indeed, treatment of **41** with 10 mol% of Pd/Au-PVP and 3 equiv. of *t*-BuOOH in $H_2O$ and $CH_3CN$ at 50 °C for 4 days gave major product C7-ketone **44** in a 62% yield and minor products $C7_{ax}$-hydroperoxide **42** (8% yield) and 7-keto-15-hydroxy **45** (10% yield) along with 14% recovery of **41**. In a larger-scale reaction using 1.5 equiv. of *t*-BuOOH, a small amount (5% yield) of $C7_{ax}$-hydroxy **43** was also isolated along with **42**, **44** (51% yield), and **45** (2% yield), where ketone **44** is the major product (Scheme 5). In a side-by-side comparison of relative reaction rates and product distributions using 5 mol% each of catalysts stabilized by **1R**, **1S** and PVP, the relative rate of reaction from **1R** was similar to that from PVP, and faster than that from **1S**. There are some degrees of match and mismatch of stereochemistry between the substrate and the chiral bimetallic nanoclusters Pd/Au, where **1R** matches with substrate **41** greater than **1S**. By increasing the amount of *t*-BuOOH to 3 equiv., oxidation of **41** with 10 mol% of Pd/Au-PVP at 50 °C for 48 h, gave only **44** and **45** in 58% and 20% yield, respectively. The spectral data of **44** are identical to those reported.[49]

Oxidation of alcohol **43** with 1 mol% of Pd/Au-PVP and 1.5 equiv. of *t*-BuOOH or IBX in DMSO gave ketone **44** (70% yield), whose spectra data are identical to those of **44** obtained from the catalytic oxidation reaction. Reduction of hydroperoxide **42** with $Na_2S_2O_5$ in 1,4-dioxane and water (9:1) gave alcohol **43** in an 85% yield. The assignment of C7-*R* configuration or α orientation of **43** is based on its $^1$H NMR spectral data, which is different

Author Manuscript Author Manuscript Author Manuscript Author Manuscript

from that reported for C7-*S* stereoisomer of **43**,[50] obtained from sodium borohydride reduction of ketone **44**.[50] The structure of **45** was assigned based on its $^{1}$H NMR, $^{13}$C NMR and mass spectra. Notably, $^{13}$C-NMR chemical shift of C-15 of **45** appears at δ 72.3 ppm, which is in agreement with the reported chemical shift of δ 72.3 ppm for hydroxyl analog, methyl 15-hydroxy-7-oxoabieta-8,11,13-trien-18-oate.[51] Likely, hydroperoxide **42** and alcohol **43** form first, which subsequently oxidize to give ketone **44**. The encouraging formation of **45** shows that acyclic alkanes can be oxidized albeit in a relative decreased reaction rate than that of cyclic alkanes under the reaction conditions.

Fermentation of the fungus *Gibberella fujikuroi* has led to the production of large quantities of gibberellic acid.[52] Subsequently, fragmentation of gibberellic acid in aqueous HCl gave 9-allogibberic acid (**46**) in a good yield.[53] Various molecules derived from **46** have shown cytotoxicity against breast cancer and colon cancer cells.[53] Because two opposite stereochemistry at C9 were reported in this reaction by the research groups,[53] we determined the structure and its relative stereochemistry by X-ray analysis. Allogibberic acid (**46**) was obtained from an aqueous-HCl treatment of gibberellic acid (see SI1, ES). After re-crystallization from diethyl ether and hexane, white crystals were obtained and the structure was solved by a single-crystal X-ray analysis and its molecular structure is revealed in Figure 4, showing C9-α-H or *R* configuration and not the described *S* configuration.[53b] The relative reaction rate of oxidation of **46** was slow due to the bulkiness of the tetracyclic structure. However, upon heating of **46** and 1 mol% of Pd/Au-PVP (25 mM aqueous solution) and 1.5 equiv. of *t*-BuOOH in concentrated $H_2O$ and $CH_3CN$ at 70 °C for 2 days, low yields of lactone **47** (16% yield) and C6-ketone **48** (5% yield) were isolated along with 38% recovery of **46** (Scheme 5).

When DMF was used as a solvent, the oxidation reaction gave a 10% yield of **47** and 3% yield of **48** as well as 32% recovered **46**. Surprisingly, treatment of **46** with 1 mol% Pd/Au-**1R** in DMF (25 mM concentration) and 1.5 equiv. of *t*-BuOOH afforded **47** and **48** in a 54% and 15% yield, respectively. Under similar reaction conditions, oxidation with 1 mol% Pd/Au-**1S** in DMF gave respectively 24% and 4% yield of **47** and **48** along with a 30% recovery of **46**. The C-H group oxidation at C9 of **46** was not found. Results indicate that oxidation reaction using **1R** polymer provided greater yields of the two products than those using **PVP** or **1S**. A match in stereochemistry of **1R** derived Pd/Au nanoclusters and **46** may enhance the relative reaction rate. Oxidation of the methyl ester derivative of **46** using $SeO_2$ and *t*-BuOOH has been described previously, and the C15-hydroxy product was reported.[53] Both lactone **47** and C6-ketone **48** have not been reported prior to this work. The structure of **47** was assigned base on its mass spectrum, $^{1}$H, $^{13}$C and 2D NOESY NMR spectra (see SI2). In the 2D NOESY spectrum, C15β-H at δ 4.53 ppm shows correlations with C11β-H at δ 1.43 ppm and one of the C17 olefinic Hs at δ 5.35 ppm (Figure 5).

Moreover, C15β-H has no correlation with C9α-H at δ 3.07 ppm, indicating C15β-H and C9α-H have opposite orientations. Hence, C15-oxygen orients at the α face. NOE (Nuclear Overhauser Effect) correlation was also found between C9α-H and C6α-H at δ 3.96 ppm. In addition, the structure of **47** was firmly established by a single-crystal X-ray analysis, shown in Figure 6. It likely forms from the C-H oxidation at C15 followed by ring

Author Manuscript Author Manuscript Author Manuscript Author Manuscript

closing with C10-carboxylic acid group. Alternatively, a complex, $RCO_2$-Pd/Au-C15, forms followed by reductive elimination to give **47**. Since the presumed C15-OH intermediate of **46** was not found, the latter proposed mechanism likely proceeds. The structure of **48** is assigned based on its spectral data, in which the C6-H signal at δ 4.01 ppm of **46** absents in the $^1$H NMR spectrum of **48**, and C9-H and C16,17-olefinic H's remain at δ 3.1, 5.06, and 4.80 ppm, respectively. The 2D NOESY showed no proton signal at C6 and low- and high-resolution mass spectra affirm the molecular formula for **48**. The $^{13}$C NMR spectrum shows the C6-carbonyl group at δ 207.0 ppm and the IR spectrum at ν 1695 $cm^{-1}$. Compound **48** likely forms from C-H group oxidation at C6 followed by decarboxylative fragmentation to give the ketone function.[54] No oxidation of the alkene function was found, and the oxidation reaction took place at C6 of **46**, adjacent to the electron-with-drawing group, carboxylic acid, is unusual. Moreover, the C-H group oxidation of cyclic aryl-α-carboxylic acid followed by decarboxylative fragmentation to form the corresponding ketone is a useful process such as ensuring the quality of active pharmaceutical ingredients.[54] Functional group manipulations of **47** and **48** will provide a library of novel derivatives for drug discovery screening.[53] To support this oxidative decarbonylation reaction, indane-1-carboxylic acid (**49**) was treated with 1 mol% Pd/Au-PVP and 1.5 equiv. of *t*-BuOOH in $CH_3CN$-$H_2O$ at 50 °C. 1-Indanone (**50**) was isolated in 40% yield along with a 45% of recovered **49**.

In a comparative study, (+)-sclareolide (**17**), an oxidation product of (−)-ambroxide (**15**), has previously reported in the oxidation by bimetallic nanoclusters Cu/Au/1$^{st}$ generation CSPVP.[5a] Expectedly, **17**, obtained from the oxidation of **15** (see Scheme 4 & Table 3), reacted very slowly with the present catalysts. Indeed, only trace amounts of oxidation products were found when **17** was treated with 5 mol% Cu/Au/PVP (or **1R**) and 2 equiv. of 30% $H_2O_2$ or Pd/Au/PVP and 2 equiv. of *t*-BuOOH at 80 °C. However, treatment of **17**, in a 1-gram-scale reaction, with 5 mol% of Cu/Au-**1R** (25 mM concentration) and 40 equiv. of 30% $H_2O_2$ in $CH_3CN$ and $H_2O$ at 90 °C for 6 days, C2-α-OH **51** (11% yield) and C2 ketone **52** (8% yield) along with C1 ketone **53** (4% yield) and **17** (57% recovery) were isolated (see a Scheme in SI1 **page 46** for the reaction equation and chemical structures). Ketone **52** was derived from the oxidation of C2-alcohol **51**. Spectral data of **51**, **52** and **53** are identical to those reported.[55] Oxidation of **17** with 5 mol% Cu/Au-PVP (25 mM) and 40 equiv. 30% $H_2O_2$ under similar reaction conditions gave similar chemical yields as those obtained from Cu/Au-**1R**. Hence, the chemical yields (a total of 33% yield) from the oxidation of **17** were slightly lower than those reported using 1$^{st}$ generation CSPVP.[5a] Significantly, when 5 mol% Cu/Au-**1S** and 40 equiv. of 30% $H_2O_2$ were used under similar reaction conditions, only 2% and 1% yield of **51** and **52**, respectively, were isolated along with 81% recovery of **17** (see **Scheme** in SI1 **page 46**). Hence, the oxidation of **17**, like **15**, showed a match with Cu/Au-**1R** nanoclusters but a mismatch with Cu/Au-**1S**.

In addition, (−)-ambroxide (**15**) was oxidized using one of the previously reported 1$^{st}$ generation chiral polymers, poly-(*N*-vinyl-5-isopropyl-pyrrolidinone; see Scheme 1, R = *i*-Pr) stabilized Cu/Au (5 mol%; 25 mM concentration) and 40 equiv. of 30% $H_2O_2$ in $CH_3CN$ and $H_2O$ at 80 °C for 3 days. Sclareolide (**17**) was isolated in 54% along with a

Author Manuscript Author Manuscript Author Manuscript Author Manuscript

31% recovery of **15** (see SI1, ES). Hence, the present catalysts provided a slightly better result than that of 1st generation CSPVP in the oxidation of **15**.

Presently, the detailed mechanism for the C-H oxidation reactions by bimetallic nanocluster/chiral and achiral polymer is unclear in part due to the unsolved bimetallic nanocluster structure. It remains undefined whether the reaction occurred at the corner or edge[56a] of the nanoclusters, on a detached metal complex by leaching[56b–d] from nanoclusters, or on small nanoclusters. Using a two-compartment membrane reactor along with transmission electron microscopy, Pd monomeric or dimeric moiety may have leached from the nanoclusters and probably responsible for the Pd-monometallic-nanocluster-catalyzed Sonogashira coupling reactions.[56d] Bimetallic nanoclusters derived from chiral polymers **1R** and **1S** showed different reactivities toward chiral ambroxide, implying that the chiral polymer involves in the oxidation reaction. A mechanism for the C-H oxidation reactions has been proposed,[5a,b] in that a $\eta^2$-peroxido $Cu^{II}$ (or peroxocopper) species,[28c,e] derived from bimetallic Cu/Au-CSPVP and $H_2O_2$, may include. A proposed mechanism for the C-H oxidation is depicted in Scheme 6, left panel. Bimetallic nanoclusters M/Au-**1R** or –PVP (where M = Cu or Pd) react with $H_2O_2$ or *t*-BuOOH to give peroxide complex **I** (R-O-O-$M^I$), which undergoes O-O bond cleavage to give metal-oxo-**1R** complex **II** (O=$M^{II}$).[11e] The oxo complex **II** abstracts a hydrogen atom from the substrate such as **33** (a representative cycloalkane) to form hydroxymetal complex **III** (HO-$M^I$) and an alkyl radical of **33**. Likely, the radical complexes with the metal atom of **III** or in a cage, and is not a free carbon radical, since no axial-oriented hydroxyl product was found. Subsequently, the alkyl radical abstracts a hydroxyl group from **III** to give oxidized product **35** and regenerate M/Au-**1R**. The metal complex may approach the C-H bond via a “concerted oxenoid oxygen insertion” mechanism,[57] leading to the insertion of an oxygen onto the C-H bond.

The weaker C-H bonds α to ether, aryl, and allyl functionalities as well as furan and tertiary C-H bond oxidized relatively faster than the secondary and primary C-H bonds. The bimetallic nanoclusters Cu/Au-polymer/$H_2O_2$ oxidative system may proceed *via* a different metals-polymer complexation than that of Pd/Au-polymer/*t*-BuOOH system, based on results of the oxidation reactions. The former may involve a tight coordinated cage system, while the latter a loose coordination or surface released or detached complex **I**.

The proposed pathways for the formation of **22** and **27** are described in Scheme 6, right panel. The oxygen of *N*-oxide **23** reacts with bimetallic nanoclusters Pd/Au-PVP to give complex **IV**, which can undergo either path **a** or **b**. In path **a**, an attack of $H_2O$ to the oxygen of Pd-O-N resulting in a cleavage of O-N bond to give product amine **22** and hydroperoxide-Pd/Au complex **V**, which dissociates to give $H_2O_2$ and Pd/Au-PVP. Path **b** involves an oxidation reaction in which the O-N bond of **IV** breaks by shifting two electrons to the electron-negative oxygen, resulting O=$Pd^{II}$ species **VI** and aminium cation **VII**. The O=$Pd^{II}$ species **VI** abstracts an α-proton of the amine function of **VII** to give HO-$Pd^I$ complex **VIII** and iminium ion **IX**. A lost of a β-proton of **IX** by **VIII** leads to vinylamine **27** and Pd/Au-PVP along with $H_2O$.

Author Manuscript Author Manuscript Author Manuscript Author Manuscript

## CONCLUSION

In summary, second-generation CSPVPs, (−)-**1R**, (+)-**1S** and (−)-**2** were synthesized from *D*-isoascorbic acid, *D*-ribose, and *L*-(*S*)-malic acid, respectively. CD spectra of the bimetallic nanoclusters showed distinct chiroptical responses, derived from chiral-polymer encapsulated nanomaterials. Efficient catalytic C-H oxidation reactions were found using catalytic amounts of bimetallic nanoclusters Cu/Au or Pd/Au stabilized by PVP or CSPVP and $H_2O_2$ or *t*-BuOOH as an oxidant. The regioselective C-H oxidations at the α-carbon of ether function of medium-sized molecule (−)-ambroxide and (*R*)-(+)-menthofuran, tertiary carbon of *N*-acetylamantadine, tertiary and secondary carbons of 1-adamantanol and *N*-acetylmemantine, and benzylic oxidation of (+)-2,9-di(*O*-pivalyl)-boldine *N*-oxide, (+)-3-*O*-pivalyl-estrone, (+)-*N*-acetyl-dehydroabietylamine, (−)-9-allogibberic acid, and (+)-sclareolide may offer various methodologies for modification of complex molecules. New oxidative reactions were discovered including selective α-C-H oxidation of the *N*-oxide function of boldine-*N*-oxide using NMO, oxidative ring closing of allogibberic acid at C-15 with the adjacent C10-carboxylic acid group, and decarboxylative oxidation at C-6 of allogibberic acid. These reactions offer new synthetic pathways in organic functional group transformation. Libraries of molecules can be produced from the aforementioned oxidative modified natural products *via* functional group manipulation for drug discovery screening.[53] This may lead to future discovery of novel drugs or improvement of pharmacokinetics of lead candidates. Catalytic oxidation of small organic molecules for assessment of enantioselectivity is underway and results will be reported in due course.

## Supplementary Material

Refer to Web version on PubMed Central for supplementary material.

## ACKNOWLEDGMENT

We are grateful to the National Institutes of Health, National Institute of General Medical Sciences (R01 GM128659) and National Science Foundation (CHE-1662705) for financial support of this research. The content is solely the responsibility of the authors and does not necessarily represent the official views of the National Institutes of Health. This material was based upon work in part supported by the National Science Foundation under 1826982 (to DHH) for the purchase of a NMR spectrometer, CHE-0923449 (to VD) and CHE-2018414 (to DHH) for the purchase of X-ray diffractometers, and NIH R01GM117259-S1 (to Ping Li) for the support of a high-resolution mass spectrometer. We thank Fei Ma, Jayaraman Aravindan and Daniel Hubin for technical assistance.

## REFERENCES

(1). Modern developments in catalysis, Hutchings G; Davidson M; Catlow R; Hardacre C; Turner N; Collier P, Ed.;Word Scientific: London, 2017, p 1 – 348.

(2). (a)Tamura M; Fujihara H, Chiral bisphosphine BINAP-stabilized gold and palladium nanoparticles with small size and their palladium nanoparticle-catalyzed asymmetric reaction. J. Am. Chem. Soc 2003, 125, 15742–15743. [PubMed: 14677954] (b)Dolamic I; Knoppe S; Dass A; Bürgi T First enantioseparation and circular dichroism spectra of Au 38 clusters protected by achiral ligands. Nat. Commun 2012, 3, 798. [PubMed: 22531183] (c)Xu Q; Kumar S; Jin S; Qian H; Zhu M; Jin R, Chiral 38-gold-atom nanoclusters: synthesis and chiroptical properties. Small 2014, 10, 1008–1014. [PubMed: 24155016]

Author Manuscript Author Manuscript Author Manuscript Author Manuscript

(3). Nishida N; Yao H; Kimura K, Chiral functionalization of optically inactive monolayer-protected silver nanoclusters by chiral ligand-exchange reactions. Langmuir 2008, 24, 2759–2766. [PubMed: 18251563]

(4). Shemer G; Krichevski O; Markovich G; Molotsky T; Lubitz I; Kotlyar AB, Chirality of silver nanoparticles synthesized on DNA. J. Am. Chem. Soc 2006, 128, 11006–11007. [PubMed: 16925401]

(5). (a)Hao B; Gunaratna MJ; Zhang M; Weerasekara S; Seiwald SN; Nguyen VT; Meier A; Hua DH, Chiral-substituted poly-N-vinylpyrrolidinones and bimetallic nanoclusters in catalytic asymmetric oxidation reactions. J. Am. Chem. Soc 2016, 138, 16839–16848. [PubMed: 27976875] (b)Zhao J; Jin R Heterogeneous catalysis by gold and gold-based bimetal nanoclusters. Nano Today 2018, 18, 86–102.(c)Baroliya PK; Chopra J; Pal T; Maiti S; Al-Thabaiti SA; Mokhtar M; Maiti B Supported metal nanoparticles assisted catalysis: a broad concept in functionalization of ubiquitous C-H bonds. ChemCatChem 2021, 13, 1–25.(d)Roduner E; Kaim W; Sarkar B; Urlacher VB; Pleiss J; Gläser R; Einicke W-D; Sprenger GA; Beifuß U; Klemm E; Liebner C; Hieronymus H; Hsu S-F; Plietker B; Laschat S Selective catalytic oxidation of C-H bonds with molecular oxygen. ChemCatChem 2013, 5, 82–112.(e)Kobayashi S; Miyamura H, Polymer-Incarcerated Metals. Higly Reactive, Recoverable, and Multifunctional Nanocluster Catalysts for Organic Synthesis. Aldrichim. Acta 2013, 46, 3–40.

(6). Lim I-IS; Mott D; Engelhard MH; Pan Y; Kamodia S; Luo J; Njoki PN; Zhou S; Wang L; Zhong CJ, Interparticle chiral recognition of enantiomers: a nanoparticle-based regulation strategy. Anal. Chem 2008, 81, 689–698.

(7). Russier-Antoine I; Bertorelle F; Kulesza A; Soleilhac A; Bensalah-Ledoux A; Guy S; Dugourd P; Brevet P-F; Antoine R, Chiral supramolecular gold-cysteine nanoparticles: Chiroptical and nonlinear optical properties. Prog. Nat. Sci.: Mater. Int 2016, 26, 455–460.

(8). Polymeric chiral catalyst design and chiral polymer synthesis, Itsuno S, Ed.; John Wiley & Sons: New Jersey, 2011, p 1 – 485.

(9). Li J; Liu Y; Ren W–M; Lu X–B Enantioselective terpolymerization of racemic and meso-epoxides with anhydrides for preparation of chiral polyesters. Proc. Nat. Acad. Sci 2020, 117, 15429–15436. [PubMed: 32581124]

(10). (a)Torchilin VP; Levchenko TS; Whiteman KR; Yaroslavov AA; Tsatsakis AM; Rizos AK; Michailova EV; Shtilman MI Amphiphilic poly-*N*-vinylpyrrolidones: synthesis, properties and liposome surface modification. Bio-materials 2001, 22, 3035–3044.(b)Okamoto Y; Nakano T Asymmetric polymerization. Chem. Rev 1994, 94, 349–372.(c)Haesuwannakij S; Kimura T; Furutani Y; Okumura K; Kokubo K; Sakata T; Yasuda H; Yakyama Y; Sakurai H The impact of the polymer chain length on the catalytic activity of poly(N-vinyl-2-pyrrolidinone)-supported gold nanoclusters. Sci. Rep 2017, 7, 9579 (8 pages). [PubMed: 28852145]

(11). (a)Gormisky PE; White MC Catalyst-controlled aliphatic C–H oxidations with a predictive model for site-selectivity. J. Am. Chem. Soc 2013, 135, 14052–14055. [PubMed: 24020940] (b)Jana S; Ghosh M; Ambule M; Gupta SS Iron complex catalyzed selective C-H bond oxidation with broad substrate scope. Org. Lett 2017, 19, 746–749. [PubMed: 28134527] (c)Doiuchi D; Uchida T Recent strategies in non-heme-type metal complex-catalyzed site-, chemo-, and enantioselective C-H oxygenations. Syn. 2021, 53, 3235–3248.(d)Costas M Site and enantioselective aliphatic C-H oxidation with bioinspired chiral complexes. Chem. Rec 2021, 21, 1–16, and references cited therein.(e)Sun Q; Sun W Catalytic enantioselective methylene C($sp^3$)-H hydroxylation using a chiral manganese complex/carboxylic acid system. Org. Lett 2020, 22, 9529–9533. [PubMed: 33300804] (f)Ottenbacher RV; Talsi EP; Bryliakov KP Highly enantioselective undirected catalytic hydroxylation of benzylic $CH_2$ groups with $H_2O_2$. J. Catal 2020, 390, 170–177. (g)Ottenbacher RV; Samsonenko DG; Nefedov AA; Talsi EP; Bryliakov KP Mn aminopyridine oxidase mimics: switching between biosynthetic-like and xenobiotic regioselectivity in C-H oxidation of (−)-ambroxide. J. Catal 2021, 399, 224–229, and references cited therein.(h)Abazid AH; Clamor N; Nachtsheim BJ An enantioconvergent benzylic hydroxylation using a chiral aryl iodide in a dual activation mode. ACS Catal. 2020, 10, 8042–8048.(i)Zheng C; You S-L Recent development of direct asymmetric functionalization of inert C–H bonds. RSC Adv. 2014, 4, 6173–6214.

Author Manuscript Author Manuscript Author Manuscript Author Manuscript

(12). Tyurina LA; Nikolaev SA; Gurevich SA; Kozhevin VM; Smirnov VV; Zanaveskin KL Selective hydrogenation of acetylene on nanosized catalysts. Catal. in Industry 2009, 1, 179–183, and references cited therein.

(13). Pauling L, The Nature of the Chemical Bond, Third Edition, Cornell University Press, Ithaca, New York, 1960.

(14). (a)Wulff G, Main-chain chirality and optical activity in polymers consisting of C-C chains. Angew. Chem., Int. Ed. Engl 1989, 28, 21–37.(b)Coates GW, Precise control of polyolefin stereochemistry using single-site metal catalysts. Chem. Rev 2000, 100, 1223–1252. [PubMed: 11749265]

(15). Hanessian S Sugar lactams. III. Synthesis of five-, six-, and seven-membered analogs. J. Org. Chem 1969, 34, 675–681.

(16). Cohen N; Banner BL; Laurenzano AJ; Carozza L 2,3-*O*-Isopropylidene-*D*-erythronolactone. Org. Synth 1985, 63, 127–130.

(17). Dirk Elend M; Fray J; Pryde D, Synthesis of 5-*O*-benzyl-2-C-β-fluoromethyl-1,2,3-tri-*O*-acetyl-*D*-ribofuranose. ARKIVOC 2006, 11, 114–127.

(18). Brice JL; Meerdink JE; Stahl SS, Formation of enamides via palladium(II)-catalyzed vinyl transfer from vinyl ethers to nitrogen nucleophiles. Org. Lett 2004, 6, 1845–1848. [PubMed: 15151429]

(19). Krishna UM; Deodhar KD; Trivedi GK Asymmetric oxidopyrylium-alkene [5+2] cycloaddition: a divergent approach for the synthesis of enantiopure oxabicycl[5.4.0]undecanes. Tetrahedron 2004, 60, 4829–4836.

(20). White JD; Hrnciar P Synthesis of polyhydroxylated pyrrolizidine alkaloids of the alexine family by tandem ring-closing metathesis-transannular cyclization. (+)-Australine. J. Org. Chem 2000, 65, 9129–9142. [PubMed: 11149861]

(21). Denmark SE; Yang S–M Total synthesis of (+)-brasilenyne. Application of an intramolecular silicon-assisted cross-coupling reaction. J. Am. Chem. Soc 2004, 126, 1243212440.

(22). (a)Cheng HN; Smith TE; Vitus DM Tacticity of poly(*N*-vinyl pyrrolidone). J. Polym. Sci.: Polym. Lett. Ed 1981, 19, 29–31.(b)Hirano T; Miyamoto Y; Amano S; Tatsumi K; Anmoto T; Kimura H; Yoshida K; Oshimura M; Ute K Hydrogen-bond-assisted isotactic-specific radical polymerization of *N*-vinyl-2-pyrrolidone with tartrate additives in toluene at low temperatures: high-resolution $^{1}$H NMR analysis. RCS Adv. 2014, 4, 53079–53089.(c)Wu J; Nakano T; Okamoto Y Asymmetric anionic polymerization of (2-fluorophenyl)(4-fluorophenyl)(2-pyridyl)methyl methacrylate leading to a helical polymer. J. Polym. Sci.: Part A: Polym. Chem 1998, 36, 2013–2019.(d)Dutta K; Brar AS Poly(vinylpyrrolidone): configurational assignments by one- and two-dimentioanl NMR spectroscopy. J. Polym. Sci., Part A: Polym. Chem 1999, 37, 3922–3928.

(23). Zhai L; Shi T; Wang H Preparation of polyvinylpyrrodinone microspheres by dispersion polymerization. Front. Chem. China 2009, 4, 83–88.

(24). (a)Zhu H; Yalcin T; Li L Analysis of the accuracy of determining average molecular weights of narrow polydispersity polymers by matrix-assisted laser desorption ionization time-of-flight mass spectrometry. J. Am. Soc. Mass Spectrom 1998, 9, 275–281. [PubMed: 9879362] (b)Frank HP; Levy GB Determination of molecular weight of polyvinylpyrrolidinone. J. Polym. Sci 1953, 10, 371–378.

(25). Toshima N; Yonezawa T, Bimetallic nanoparticlesnovel materials for chemical and physical applications. New J. Chem 1998, 22, 1179–1201.

(26). (a)Hou W; Dehm NA; Scott RWJ Alcohol oxidations in aqueous solutions using Au, Pd, and bimetallic AuPd nanoparticle catalysts. J. Catal 2008, 253, 22–27.(b)Scott RWJ; Wilson OM; Oh S–K; Kenik EA; Crooks RM Bimetallic palladium-gold dendrimer-encapsulated catalysts. J. Am. Chem. Soc 2004, 126, 15583–15591. [PubMed: 15563188] (c)Harada M; Asakura K; Toshima N Catalytic activity and structural analysis of polymer-protected Au/Pd bimetallic clusters prepared by the successive reduction of $HAuCl_4$ and $PdCl_2$. J. Phys. Chem 1993, 97, 5103–5114.

(27). (a)Yao H; Kobayashi R Chiral monolayer-protected Au-Pd bimetallic nanoclusters: effect of palladium doping on their chiroptical responses. J. Colloid Interface Sci 2014, 419, 1–8. [PubMed: 24491322] (b)Oh HS; Liu S; Jee H; Baev A; Swihart MT; Prasad PN Chiral poly(fluorine-alt-benzothiadiazole) (PFBT) and nanocomposites with gold nanoparticles:

Author Manuscript Author Manuscript Author Manuscript Author Manuscript

plasmonically and structurally enhanced chirality. J. Am. Chem. Soc 2010, 132, 17346–17348. [PubMed: 21090623]

(28). (a)McGuirl AM; Dooley DM Copper-containing oxidases. Curr. Opin. Chem. Biol 1999, 3, 138–144. [PubMed: 10226045] (b)Roiban G-D; Agudo R; Reetz MT Cytochrome P450 catalyzed oxidative hydroxylation of achiral organic compounds with simultaneous creation of two chirality centers in a single C-H activation step. Angew. Chem. Int. Ed 2014, 53, 8659–8663.(c)Culpepper MA; Rosenzweig AC Architecture and active site of particulate methane monooxygenase. Crit. Rev. Biochem. Mol. Biol 2012, 47, 483–492. [PubMed: 22725967] (d)See YY; Herrmann AT; Aihara Y; Baran PS, Scalable C–H oxidation with copper: synthesis of polyoxypregnanes. J. Am. Chem. Soc 2015, 137, 13776–13779. [PubMed: 26466196] (e)Wendlandt AE; Suess AM; Stahl SS Copper-catalyzed aerobic oxidative C-H functionalizations: trends and mechanistic insights. Angew. Chem. Int. Ed 2011, 50, 11062–11087.

(29). (a)Margaros I; Montagnon T; Vassilikogiannakis G Spiroperoxy lactones from furans in one pot: synthesis of (+)-premnalane A. Org. Lett 2007, 9, 5585–5588. [PubMed: 18027962] (b)Barrero AF; Alvarez-Manzaneda EJ; Altarejos J; Salido S; Ramos JM Synthesis of ambrox® from (−)-sclareol and (+)-cis-abienol. Tetrahedron 1993, 49, 10405–10412.

(30). (a)Seto H; Yoshida K; Yoshida S; Shimizu T; Seki H; Hoshino M Oxidation of ethers to esters by photo-irradiation with benzil and oxygen. Tetrahedron Lett. 1996, 37, 4179–4182.(b)Laudadio G; Govaerts S; Wang Y; Ravelli D; Koolman HF; Fagnoni M; Djuric SW; Noel T Selective C($sp^3$)-H aerobic oxidation enabled by decatungstate photocatalysis in flow. Angew. Chem. Int. Ed 2018, 57, 4078–4082.(c)Chen MS; White MC Combined effects on selectivity in Fe-catalyzed methylene oxidation. Science 2010, 327, 566–571. [PubMed: 20110502]

(31). (a)Bates RW; Sridhar S A synthesis of (−)-mintlactone. J. Org. Chem 2008, 73, 8104–8105. [PubMed: 18811204] (b)Patel RM; Puranik VG; Argade NP Regio- and stereoselective selenium dioxide allylic oxidation of (*E*)-dialkyl alkylidenesuccinates to (*Z*)-allylic alcohols: synthesis of natural and unnatural butenolides. Org. Biomol. Chem 2011, 9, 6312–6322. [PubMed: 21792406] (c)Kotzabasaki V; Vassilikogiannakis G; Stratakis M Regiocontrolled synthesis of γ-hydroxybutenolides via singlet oxygen-mediated oxidation of 2-thiophenyl furans. J. Org. Chem 2016, 81, 4406–4411. [PubMed: 27128450]

(32). (a)Woodward RB; Eastman RH The autoxidation of menthofuran. J. Am. Chem. Soc 1950, 72, 399–403.(b)Takahashi K; Someya T; Muraki S; Yoshida T A new keto-alcohol, (−)-mintlactone, (+)-isomintlactone and minor components in peppermint oil. Agric. Biol. Chem 1980, 44, 1535–1543.

(33). (a)Horinaka A; Naya K The transformations of terpene ketones by oxygen. I. The autoxidation of fukinone. Bull. Chem. Soc. Jpn 1979, 52, 1964–1966.(b)Bao J; Tian H; Yang P; Deng J; Gui J Modular synthesis of functionalized butenolides by oxidative furan fragmentation. Eur. J. Org. Chem 2020, 339–347.

(34). Thomassen D; Knebel N; Slattery JT; McClanahan RH; Nelson SD Reactive intermediates in the oxidation of menthofuran by cytochromes P-450. Chem. Res. Toxicol 1992, 5, 123–130. [PubMed: 1581528]

(35). (a)Pech B; Bruneton J Alcaloides du laurier noble, Laurus nobilis. J. Nat. Prod 1982, 45, 560–563.(b)Lee S–S; Lai Y–C; Chen C–K; Tseng L–H; Wang C–Y Characterization of isoquinoline alkaloids from *Neolitsea sericea var. aurata* by HPLC-SPE-NMR. J. Nat. Prod 2007, 70, 637–642. [PubMed: 17388628]

(36). Zhao H; Xu H; Qiao S; Lu C; Wang G; Liu M; Guo B; Tan Y; Ju D; Xiao C Boldine isolated from Litsea cubeba inhibits bond resorption by suppressing the osteoclast differentiation in collagen-induced arthritis. Int. Immunopharm 2017, 51, 114–123.

(37). Huang W–J; Chen C–H; Singh OV; Lee S–L; Lee S–S A facile method for the synthesis of glaucine and norglaucine from boldine. Syn. Commun 2002, 32, 3681–3686.

(38). Pati K; Liu R–S Efficient syntheses of α-pyridones and 3(2*H*)-isoquinolones through ruthenium-catalyzed cycloisomerization of 3-en-5-ynyl and *o*-alkynylphenyl nitrones. Chem. Commun 2009, 5233–5235.

(39). Chung T–H; Li C–F; Lee H–Z; Wen Y–C Direct conversion of 1-(2-bromobenzoyl)isoquinolines to dibenzo[de,g]quinolin-7-ones via reductive photocyclization. J. Org. Chem 2013, 78, 4974–4984. [PubMed: 23611299]

Author Manuscript Author Manuscript Author Manuscript Author Manuscript

(40). (a)Cava MP; Srinivasan M Conversion of aporphines into *N*-noraporphine alkaloids. J. Org. Chem 1972, 37, 330–332. [PubMed: 5013355] (b)Craig JC; Purushothaman KK Structure of the compound from trimethylamine oxide and sulfur dioxide: an amine oxide rearrangement. Tetrahedron Lett. 1969, 60, 5305–5306.

(41). Mitsukura K; Sakamoto H; Kubo H; Yoshida T; Nagasawa T Bioconversion of 1-adamantanol to 1,3-adamantanediol using Streptomyces sp. SA8 oxidation system. J. Biosci. Bioeng 2010, 109, 550–553. [PubMed: 20471592]

(42). Sarkar MR; Hall EA; Dasgupta S; Bell SG The use of directing groups enables the selective and efficient bio-catalytic oxidation of unactivated adamantyl C-H bonds. ChemistrySelect 2016, 1, 6700–6707.

(43). (a)Blanchet PJ; Metman LV; Chase TN Renaissance of amantadine in the treatment of Parkinson's disease. Adv. Neurol 2003, 91, 251–257. [PubMed: 12442683] (b)Fresno N; Perez-Fernandez R; Goicoechea C; Alkorta I; Fernandez-Carvajal a.; de la Torre-Martinez R; Quirce S; Ferrer-Montiel A; Martin MI; Goya P; Elguero J Adamantyl analogues of paracetamol as potent analgesic drugs via inhibition of TRPA1. PloS ONE 2014, 9, e113841, 16 pages. [PubMed: 25438056] (c)Jin X; Liu Z; Guo B; Zhang G; Zhang Z; Xu L; Wang Y; Sun Y A promising dual-functional neuroprotective derivative of memantine. J. Pharm. Biomed. Sci 2016, 6, 392–398.

(44). del Río-Sancho S Diagnosis and management in dementia; in "The neuroscience of dementia"; Elsevier Inc., 2020, 1, 511–527.

(45). (a)Blanpied TA; Clarke RJ; Johnson JW Amantadine inhibits NMDA receptors by accelerating channel closure during channel block. J. Neurosci 2005, 25, 3312–3322. [PubMed: 15800186] (b)Glasgow NG; Povyssheva NV; Azofeifa AM; Johnson JW Memantine and ketamine differentially alter NMDA Receptor Desensitization. J. Neurosci 2017, 37, 9686–9704. [PubMed: 28877967]

(46). Ottenbacher RV; Talsi EP; Rybalova T; Bryliakov KP Enantioselective benzylic hydroxylation of arylalkanes with $H^2O^2$ in fluorinated alcohols in the presence of chiral Mn aminopyridine complexes. ChemCatChem 2018, 10, 5323–5330.

(47). Kirk DN; Slade CJ Synthesis of the 11-(hydrogen succinate) and 11-(β-D-glucopyranosiduronic acid) derivative of estra-1,3,5(10)-triene-3,11α,17β-triol. J. Chem. Soc. Perkin Trans 1 1984, 2595–2596.

(48). Gonzalez MA Aromatic abietane diterpenoids: their biological activity and synthesis. Nat. Prod. Rep 2015, 32, 684–704. [PubMed: 25643290]

(49). Dea-Ayuela MA; Bibao-Ramos P; Bolas-Fernandez F; Gonzalez-Cardenete MA Synthesis and antileishmanial activity of C7- and C12-functionalized dehydroabietylamine derivatives. Eur. J. Med. Chem 2016, 121, 445–450. [PubMed: 27318121]

(50). Liu C–X; Lin Z–X; Zhou A Design, synthesis, cytotoxicities and DNA cleavage activities of dibenzoxepine and isoquinoline derivatives starting from dehydroabietylamine. J. Asian Nat. Prod. Res 2016, 18, 1169–1177. [PubMed: 27696913]

(51). Kolsi LE; Krogerus S; Brito V; Ruffer T; Lang H; Yli-Kauhaluoma J; Silvestre SM; Moreira VM Regiose-lective benzylic oxidation of aromatic abietanes: application to the semisynthesis of the naturally occurring picealactones A, B and C. ChemistrySelect 2017, 2, 7008–7012.

(52). Werle LB; Abaide ER; Felin TH; Kuhn KR; Tres MV; Zabot GL; Kuhn RC; Jahn SL; Mazutti MA Gibberellic acid production from Gibberella fujikuroi using agro-industrial residues. Biocat. Agricul. Biotech 2020, 25, 101608, 5 pages.

(53). (a)Wu M–J; Wu D–M; Chen J–B; Zhao J–F; Gong L; Gong Y–X; Li Y; Yang X-D; Zhang H Synthesis and anti-proliferative activity of allogibberic acid derivatives containing 1,2,3-triazole pharmacophore. Bioorg. & Med. Chem. Lett 2018, 28, 2543–2549. [PubMed: 29884535] (b)Zhang H; Wu M–J; Li Y; He Y; Chen J–B; Yang X-D; Chen W; Gong Y Gibberellin-like compound, preparation method thereof, pharmaceutical composition, uses and intermediate thereof. WO 2019/184772 A1, 2019, 86 pages.

(54). Gangadurai C; Illa GT; Reddy DS $FeCl_3$-catalyzed oxidative decarboxylation of aryl/heteroaryl acetic acids: preparation of selected API impurities. Org. Biomol. Chem 2020, 18, 8459–8466. [PubMed: 33057544]

Author Manuscript Author Manuscript Author Manuscript Author Manuscript

(55). Canta M; Font D; Gomez L; Ribas X; Costas M The iron(II) complex [Fe($CF_3SO_3$)$_2$(mcp)] as a convenient, readily available catalyst for the selective oxidation of methylenic sites in alkanes. Adv. Synth. Catal 2014, 356, 818–830.

(56). (a)Astruc D; Lu F; Aranzaes JR, Nanoparticles as recyclable catalysts: the frontier between homogeneous and heterogeneous catalysis. Angew. Chem., Int. Ed 2005, 44, 7852–7872. (b)Ananikov VP; Beletskaya IP Toward the ideal catalyst: from atomic centers to a “cocktail” of catalysts. Organomet. 2012, 31, 1595–1604.(c)Yasukawa T; Miyamura H; Kobayashi S Chiral ligand-modified metal nanoparticles as unique catalysts for asymmetric C-C bond-forming reactions: how are active species generated: ACS Catal. 2016, 6, 7979–7988.(d)Thathagar MB; ten Elshof JE; Rothenberg G Pd nanoclusters in C-C coupling reactions: proof of leaching. Angew. Chem. Int. Ed 2006, 45, 2886–2890.

(57). Bravo A; Fontana F; Fronza G; Minisci F; Zhao L, Molecule-induced homolysis versus “concerted oxenoid oxygen insertion” in the oxidation of organic compounds by dimethyldioxirane. J. Org. Chem 1998, 63, 254–263.

Author Manuscript Author Manuscript Author Manuscript Author Manuscript

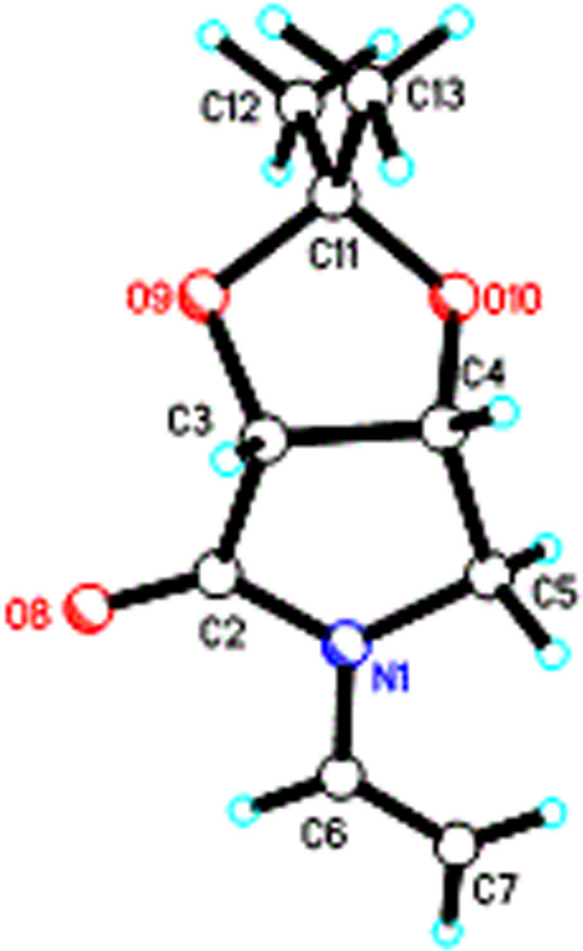


**Figure 1.**
ORTEP representation of (−)-**6** obtained from a single-crystal X-ray analysis. Displacement ellipsoids are drawn at the 50% probability level.

Author Manuscript Author Manuscript Author Manuscript Author Manuscript

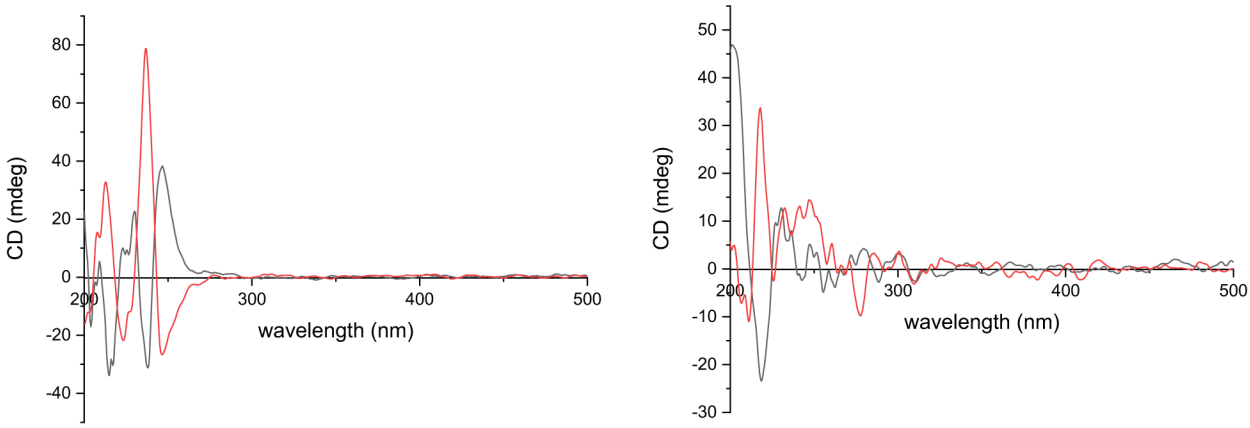


**Figure 2.**

Left panel: Overlay of circular dichroism (CD) spectra of (−)-Cu:Au (3:1)/−**1R** (black line) and (+)-Cu:Au (3:1)/−**1S** (red line). Right panel: (−)-Pd:Au (3:1)/−**1R** (black line) and (+)-Pd:Au (3:1)/−**1S** (red line) in 1.5 mM in deionized water.

Author Manuscript Author Manuscript Author Manuscript Author Manuscript

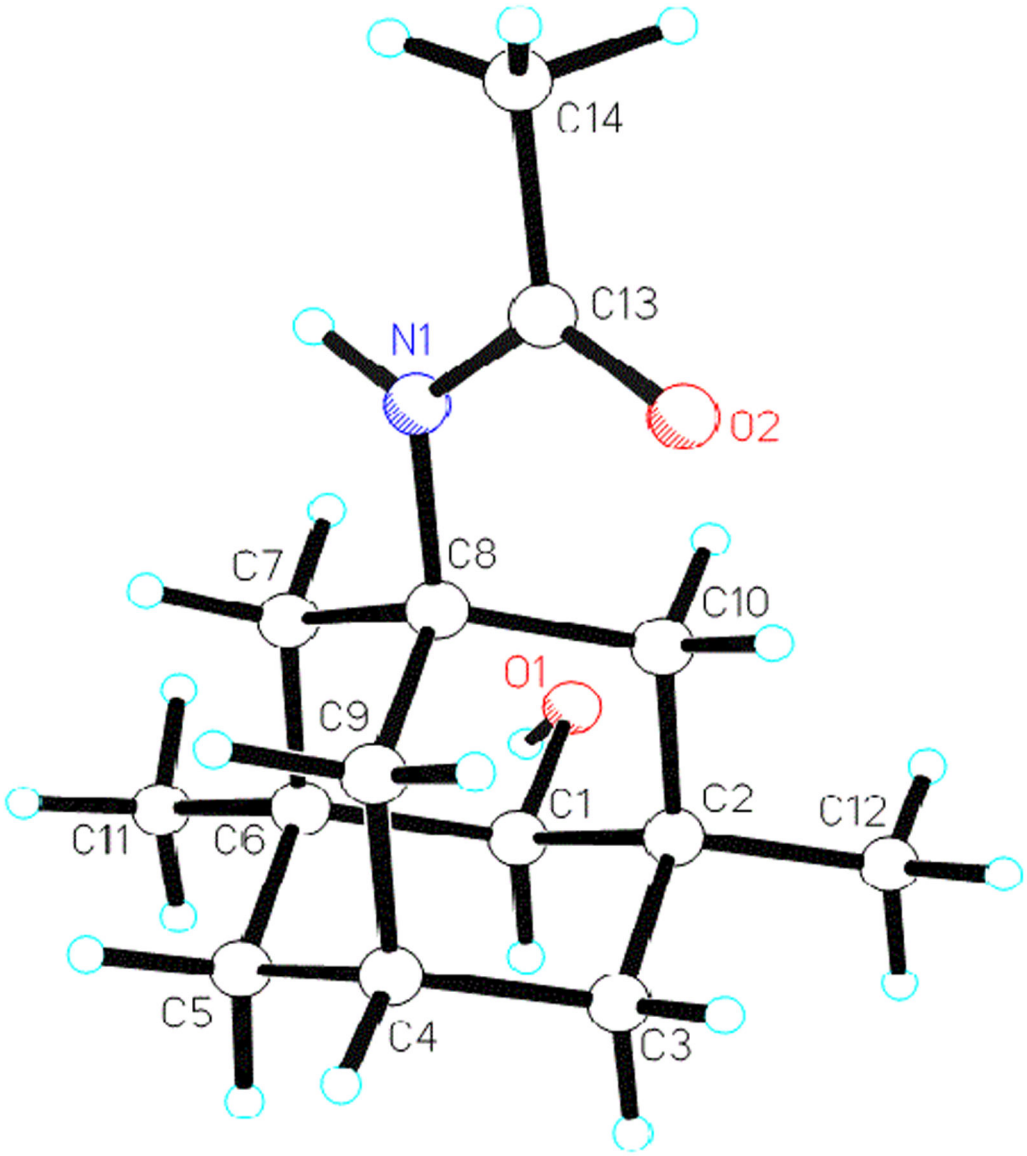


**Figure 3.**

ORTEP representation of *N*-4-hydroxy-3,5-dimethyl-adamantan-1-yl acetamide (**35**), obtained from a single-crystal X-ray analysis. Displacement ellipsoids are drawn at the 50% probability level.

Author Manuscript Author Manuscript Author Manuscript Author Manuscript

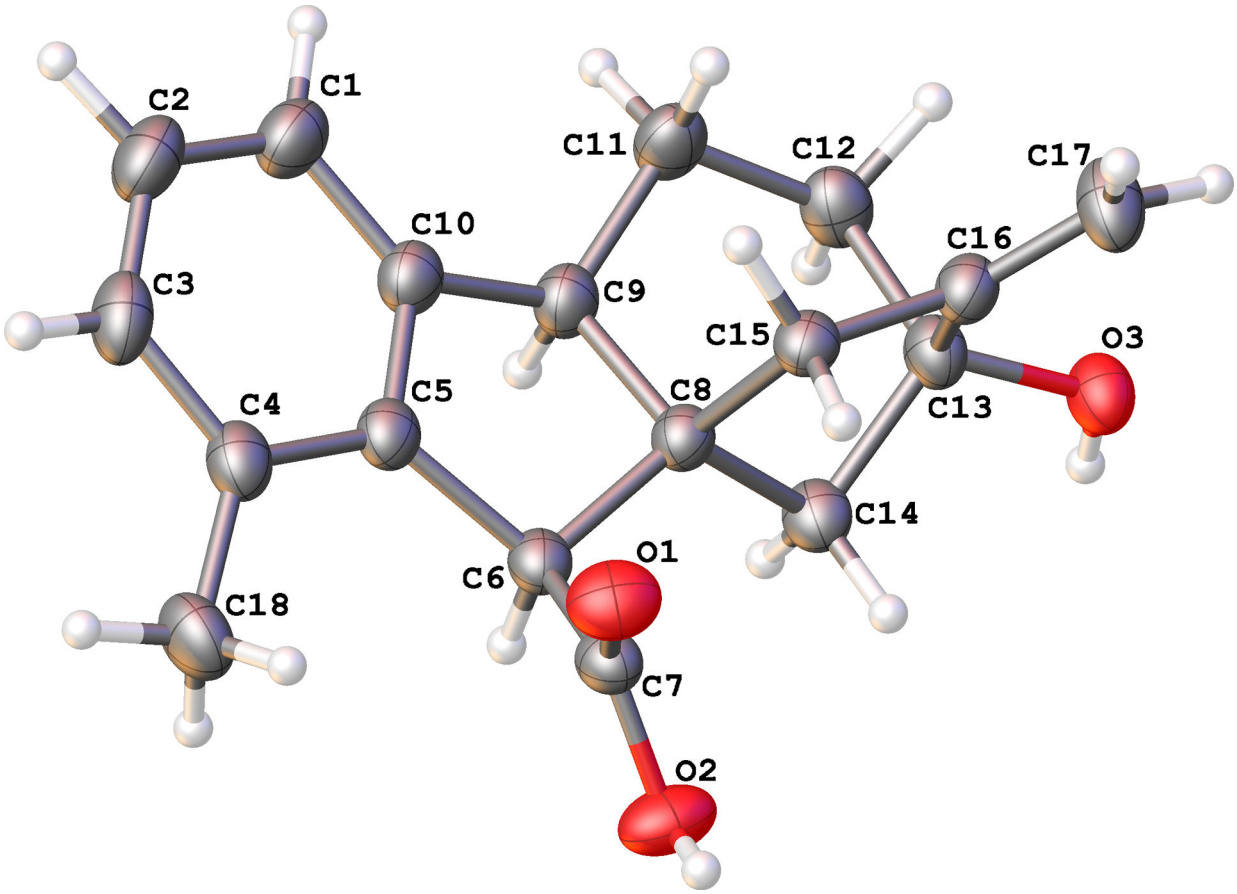


**Figure 4.**

ORTEP representation of allogibberic acid (**46**), obtained from a single-crystal analysis. Displacement ellipsoids are drawn at the 50% probability level.

Author Manuscript Author Manuscript Author Manuscript Author Manuscript

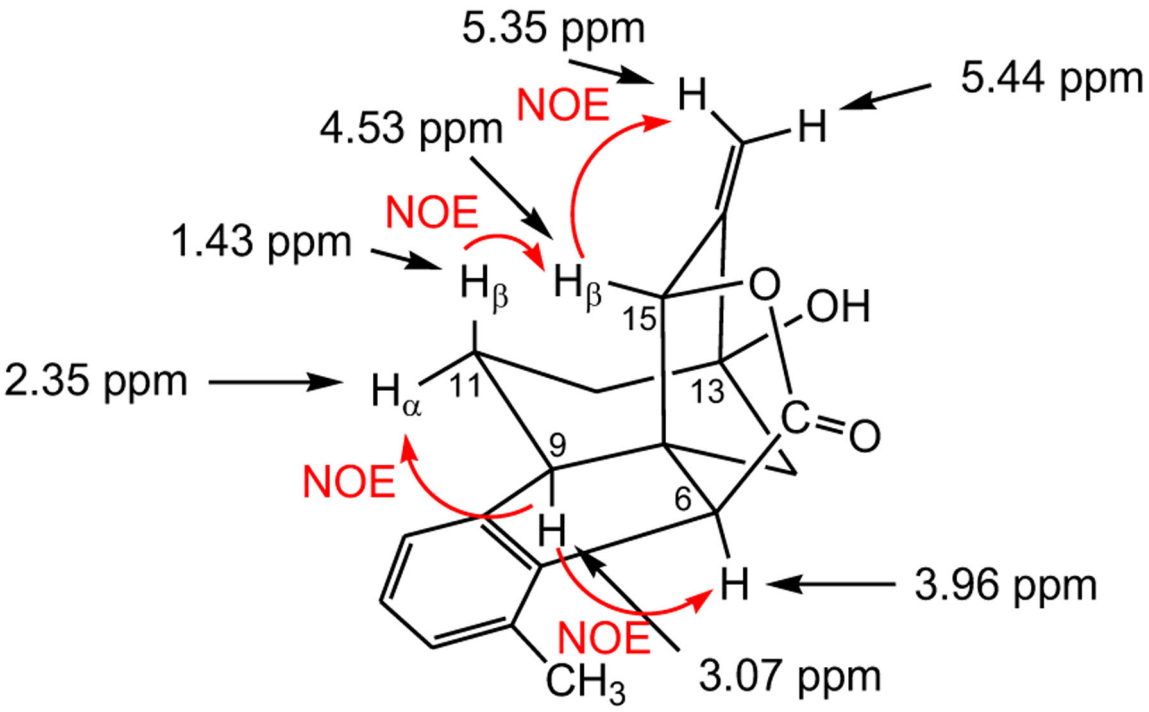


**Figure 5.**
NOE correlations from 2D NOESY NMR spectrum of compound **47**.

Author Manuscript Author Manuscript Author Manuscript Author Manuscript

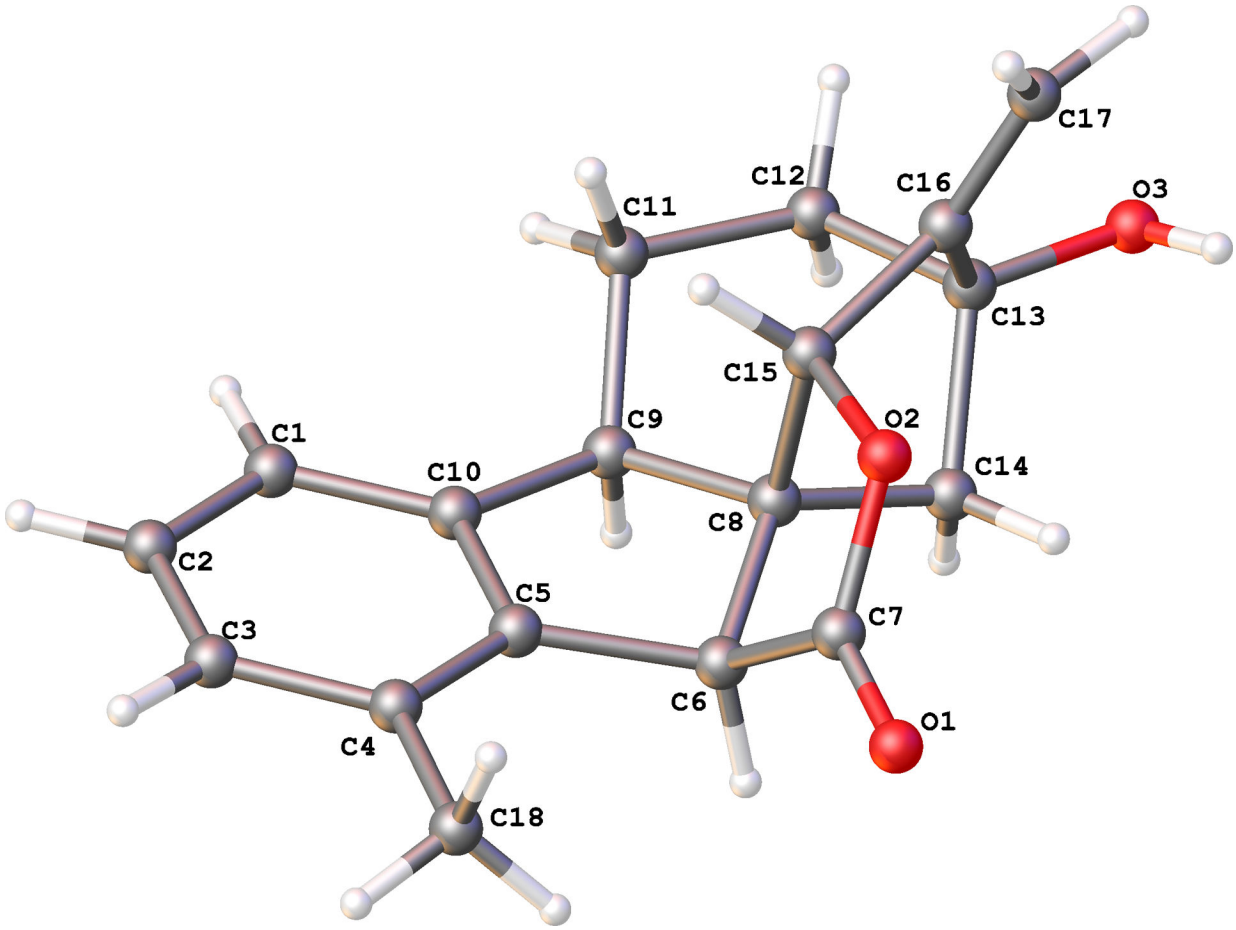


**Figure 6.**

ORTEP representation of lactone **47**, obtained from a single-crystal X-ray analysis. Displacement ellipsoids are drawn at the 50% probability level.

Author Manuscript Author Manuscript Author Manuscript Author Manuscript

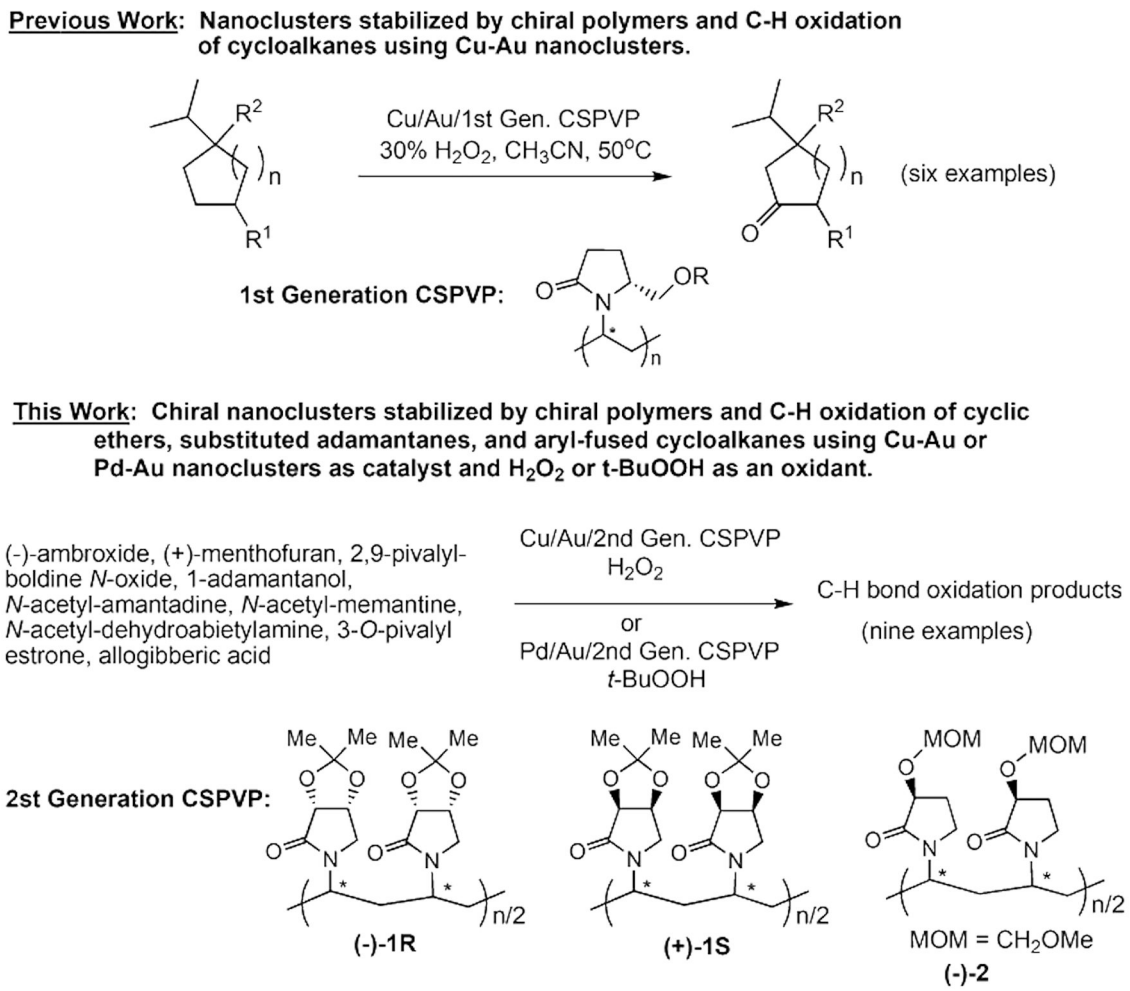


**Scheme 1.**

Previous and present works using bimetallic nanoclusters-stabilized by polymers.

Author Manuscript Author Manuscript Author Manuscript Author Manuscript

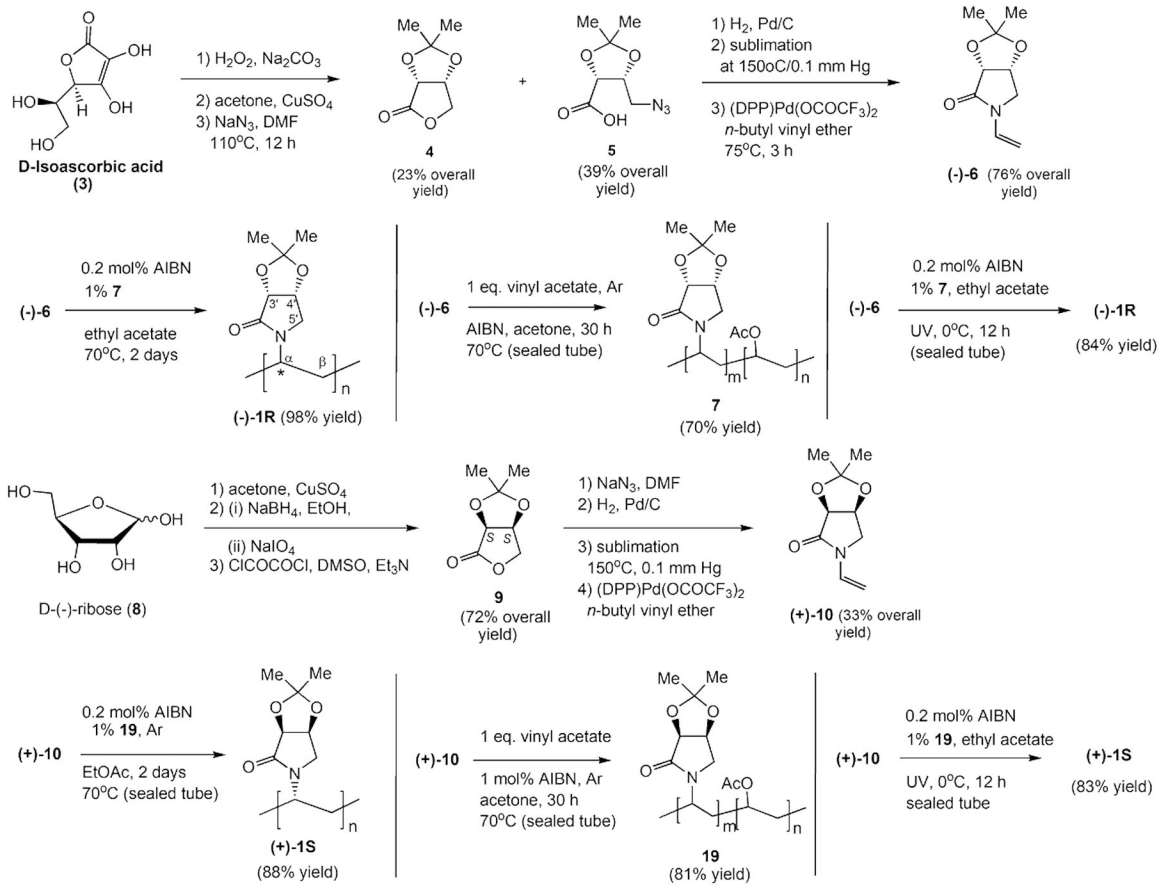


**Scheme 2.**

Syntheses of vinyl lactams (−)-6 and (+)-10, and CSPVP (−)-1R and (+)-1S

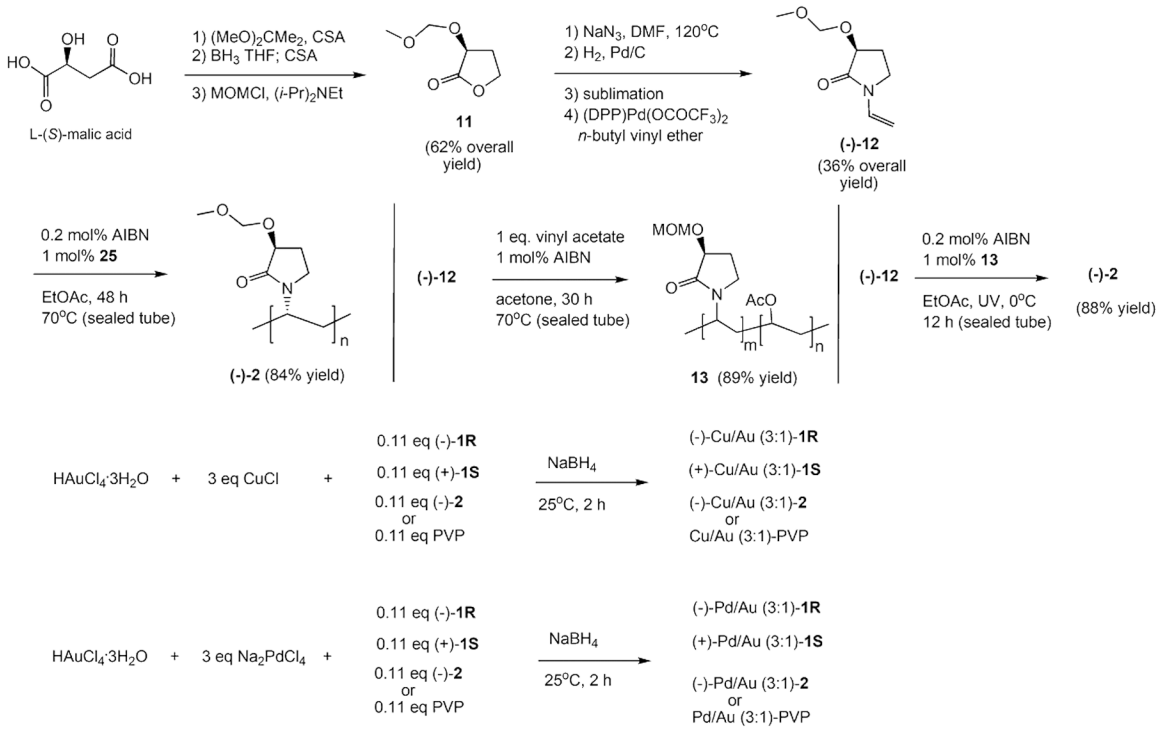


**Scheme 3.**

Synthesis of vinyl lactam (−)-13 and CSPVP (−)-2 and preparation of chiral bimetallic nanoclusters



Author Manuscript Author Manuscript Author Manuscript Author Manuscript

Author Manuscript Author Manuscript Author Manuscript Author Manuscript

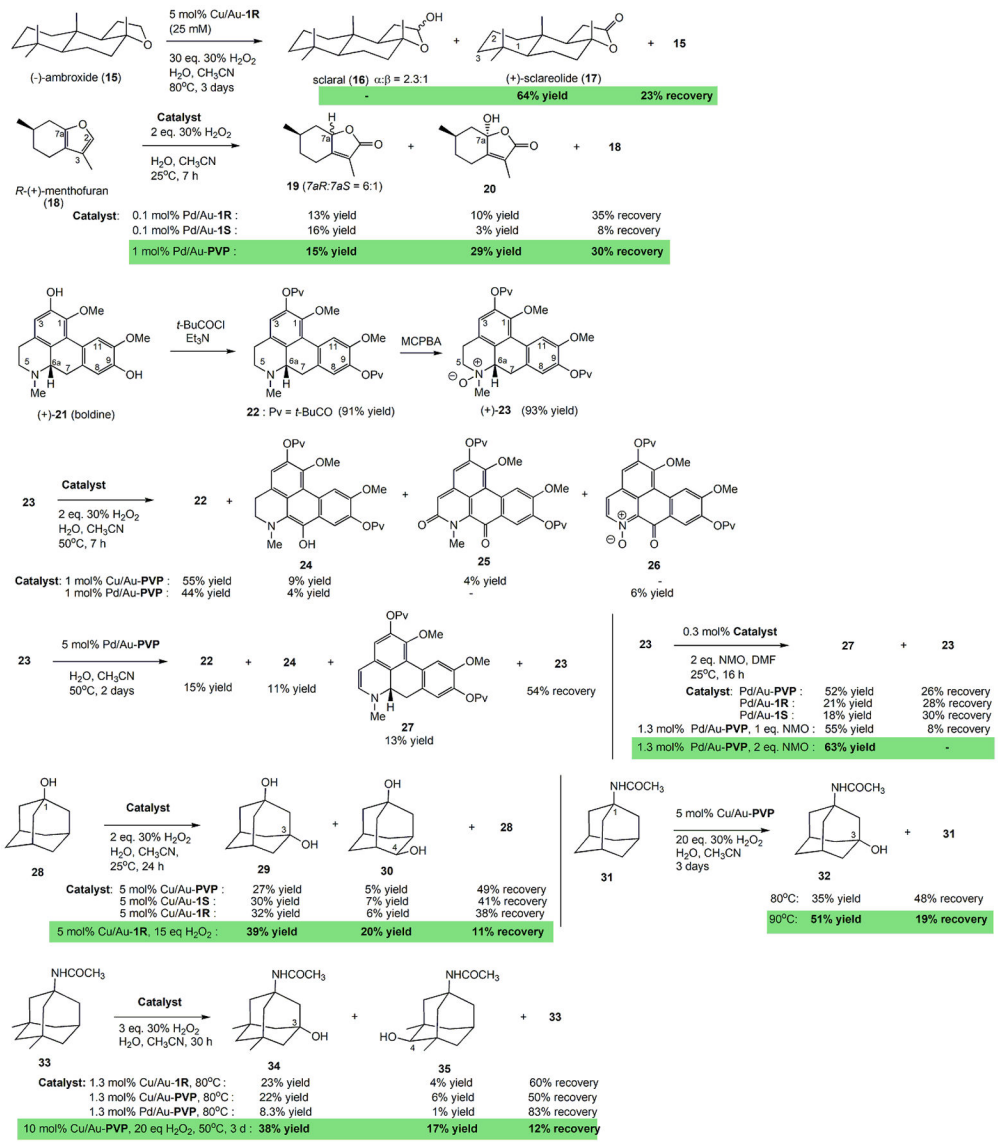


**Scheme 4.**

Catalytic C-H bond oxidations of complex molecules using bimetallic nanoclusters as catalysts and 30% $H_2O_2$ or NMO as an oxidant. Note: For 1 mole of substrate, the use of 2 eq. of 30% $H_2O_2$ is 2 mole of 30% $H_2O_2$.

Author Manuscript Author Manuscript Author Manuscript Author Manuscript

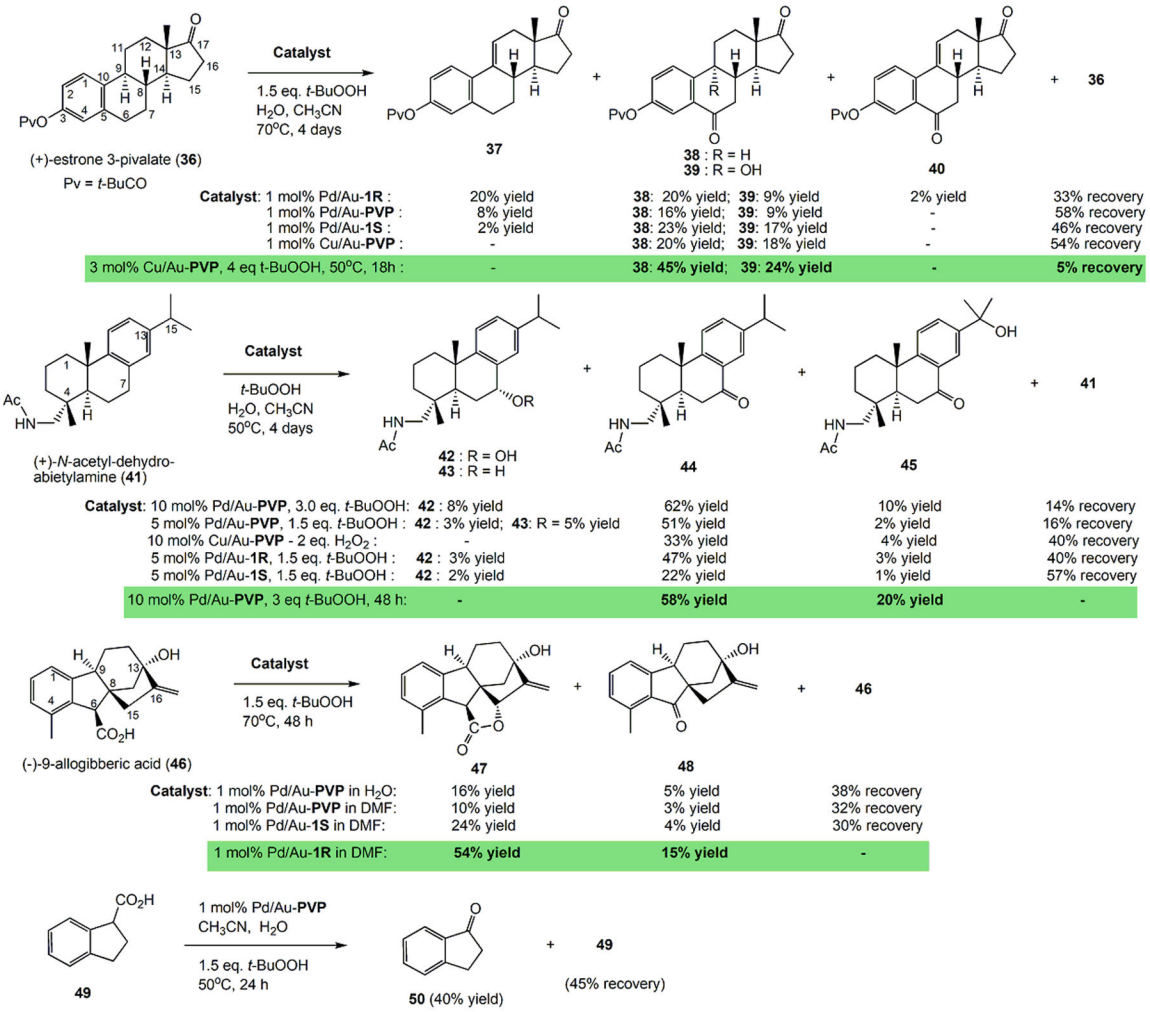


**Scheme 5.**

Catalytic C-H bond oxidations of complex molecules using bimetallic nanoclusters as catalysts and *t*-BuOOH as an oxidant.

Author Manuscript Author Manuscript Author Manuscript Author Manuscript

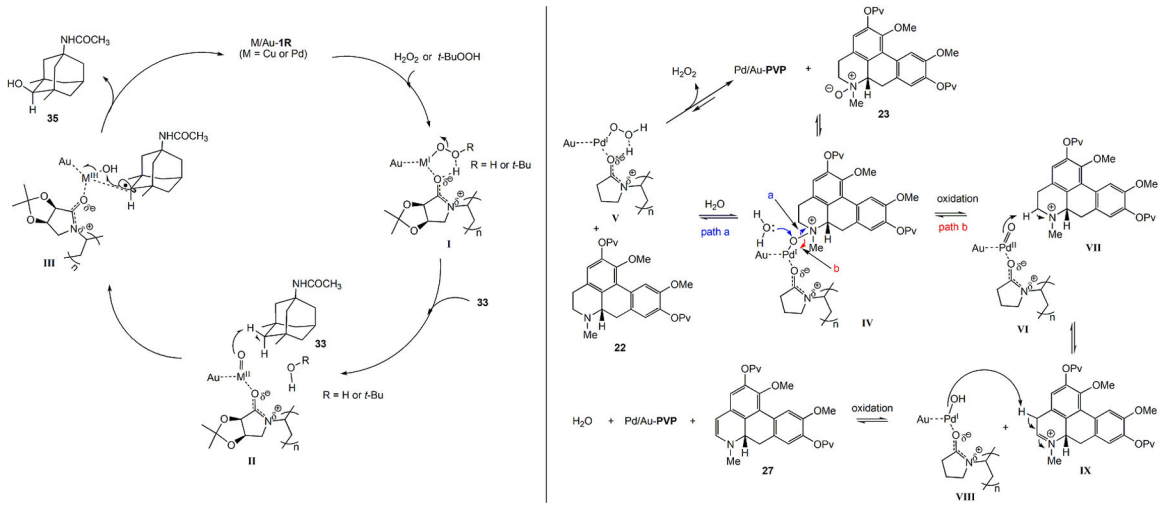


**Scheme 6.**

Proposed mechanism for C-H oxidation with bimetallic nanoclusters and mechanism for the formations of 22 and 27.

Author Manuscript Author Manuscript Author Manuscript Author Manuscript

**Table 1.**

Number average molecular weight ($M_n$), weight average molecular weights ($M_w$), polydispersity index (PI), numbers of monomer units (n) in the polymer, and specific rotations of CSPVP (−)-**1R**, (+)-**1S**, and (−)-**2**, using 0.2 mol% AIBN in the polymerization reactions.

| Entry | CSPVP, reaction conditions | MW from HRMS | Polydispersity index (PI = $M_w/M_n$ | n (number of monomer units) | $[\alpha]_D^{22}$ (c = 0.5; $CHCl_3$) |
|---|---|---|---|---|---|
| 1 | **(−)-1R**, 70 °C | $M_n$= 85,232.5236<br>$M_w$=89,051.4707 | 1.04 | 486 | −42.7 |
| 2 | **(−)-1R**, UV, 0 °C | $M_n$ =51,795.4751<br>$M_w$=53,547.9798 | 1.03 | 292 | −38.0 |
| 3 | **(+)-1S**, 70 °C | $M_n$=74,449.8841<br>$M_w$=80,021.809 | 1.07 | 437 | +35.3 |
| 4 | **(+)-1S**, UV, 0 °C | $M_n$= 46,417.5788<br>$M_w$=48,459.1355 | 1.04 | 283 | +32.4 |
| 5 | **(−)-2**, 70 °C | $M_n$=57,297.4884<br>$M_w$=59,871.4884 | 1.04 | 350 | −168.0 |
| 6 | **(−)-2**, UV, 0 °C | $M_n$ = 28,737.377<br>$M_w$=30,969.1485 | 1.08 | 181 | −155. 0 |

Author Manuscript

Author Manuscript

Author Manuscript

Author Manuscript

**Table 2.**

Results of molecular weight measurements and intrinsic viscosity of CSPVPs and PVPs prepared by thermal reaction in ethyl acetate at 70 °C and different mol% of AIBN in sealed tubes.

| Entry | Polymers (amount of AIBN used) | MW obtained from HRMS | n (number of monomer units) | Intrinsic viscosity, [η] (mL/g) |
|---|---|---|---|---|
| 1 | (−)-**1R** (0.1 mol%) | $M_n$ = 130,512.278<br>$M_w$ = 135,323.932 | 739 | 49.90 |
| 2 | (−)-**1R** (0.2 mol%) | $M_n$ = 85,232.5236<br>$M_w$ = 89,051.4707 | 486 | 44.44 |
| 3 | (−)-**1R** (0.4 mol%) | $M_n$ = 45,580.4601<br>$M_w$ = 48,038.7775 | 262 | 40.16 |
| 4 | (+)-**1S** (0.2 mol%) | $M_n$ = 74,449.8841<br>$M_w$ = 80,021.809 | 437 | 44.10 |
| 5 | (−)-**2** (0.2 mol%) | $M_n$ = 57,297.4884<br>$M_w$ = 59,871.4884 | 350 | 27.75 |
| 6 | PVP (0.1 mol%) | $M_n$ = 59,359.159<br>$M_w$ = 59,611.538 | 537 | 41.67 |
| 7 | PVP (0.2 mol%) | $M_n$ = 37,341.4092<br>$M_w$ = 42,946.4619 | 386 | 34.04 |
| 8 | PVP (0.4 mol%) | $M_n$ =30,936.9243<br>$M_w$ = 32,678.9437 | 294 | 26.4 |

Author Manuscript Author Manuscript Author Manuscript Author Manuscript

**Table 3.**

Catalytic oxidations of (−)-ambroxide (**15**) with monometallic or bimetallic nanoclusters and 2 equivalents of 30% $H_2O_2$ in acetonitrile-water (1:1) (10 mM) at 80 °C for 3 days.

| Entry | mol% of Catalysts (3:1 of bimetallic nanoclusters or monoclusters | Product(s), (isolated yields) | Recovered 15 |
|---|---|---|---|
| 1 | None | - | 88% |
| 2 | 5% Au-PVP | - | 87% |
| 3 | 5% Cu-PVP | - | 87% |
| 4 | 5% Pd-PVP | **16** (1%) and **17** (2%) | 83% |
| 5 | 5% Pd/Au-PVP | **16** (1%) and **17** (14%) | 72% |
| 6 | 5% Cu/Au-PVP | **17** (20%) | 67% |
| 7 | 5% Cu/Au-**1R** | **17** (37%) | 51% |
| 8 | 5% Cu/Au-**1S** | **17** (1%) | 84% |
| 9 | 5% Cu/Au-**2** | **17** (2%) | 83% |
| 10 | 5% Cu/Au-**1R** (25 mM)[a] | **17** (64%) | 23% |

[a] 40 equivalents of 30% $H_2O_2$ were used.